Observational Cosmology

(C. Porciani / K. Basu)

Lecture 9

Cosmology with galaxy clusters

Course website:

http://www.astro.uni-bonn.de/~kbasu/ObsCosmo

Questions?

X-ray observation

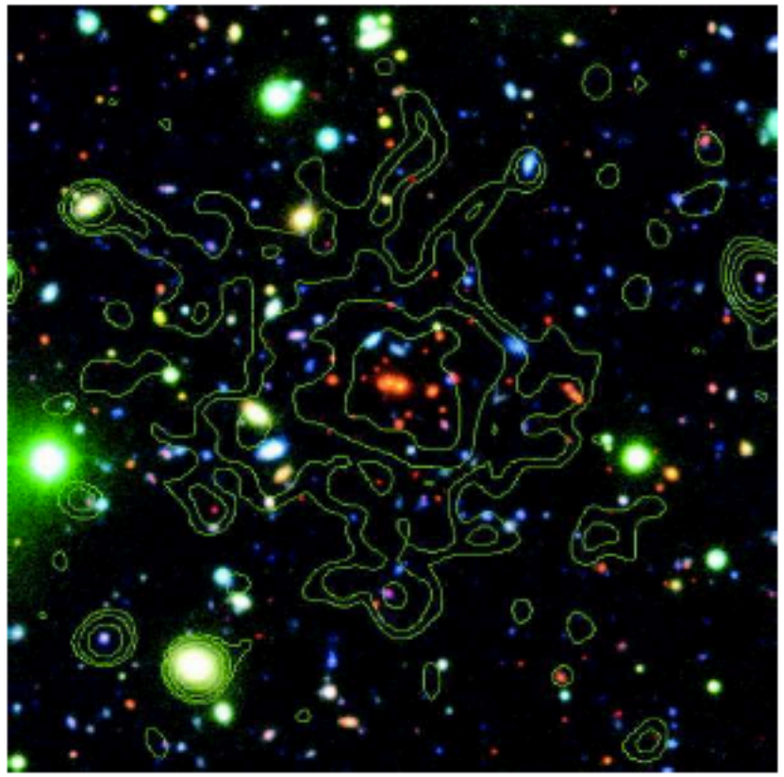

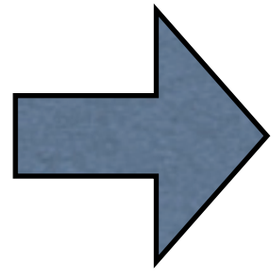

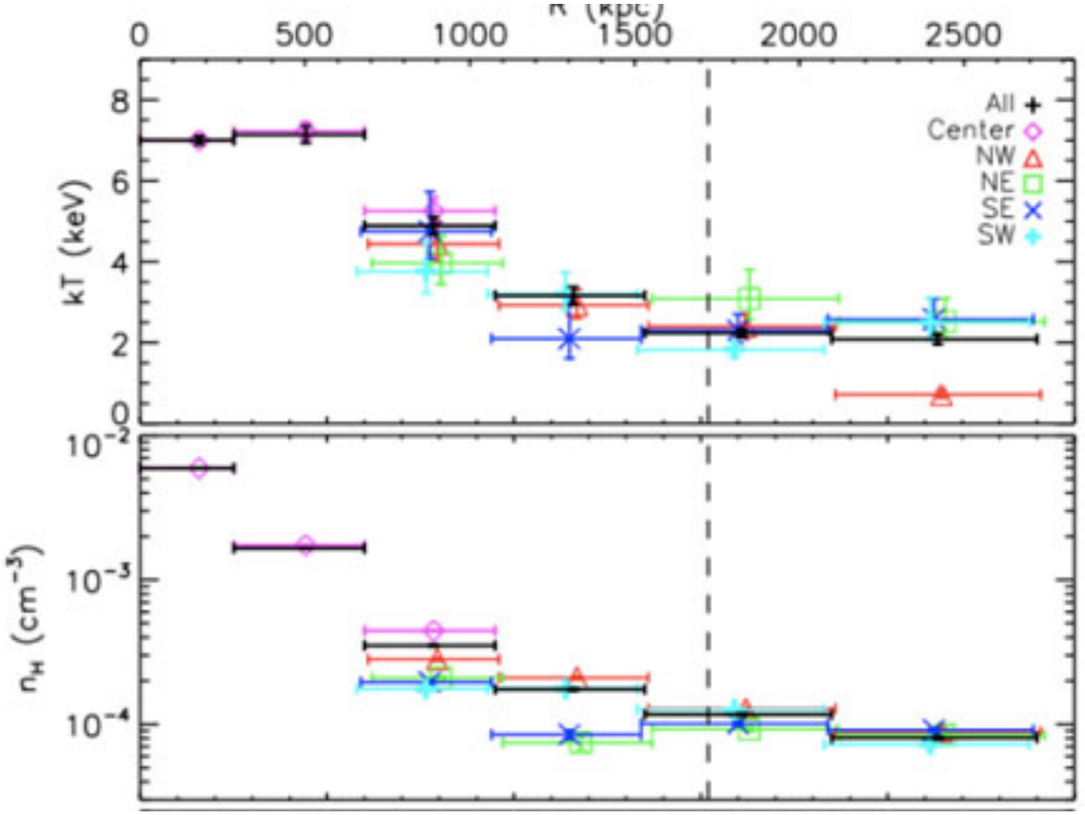

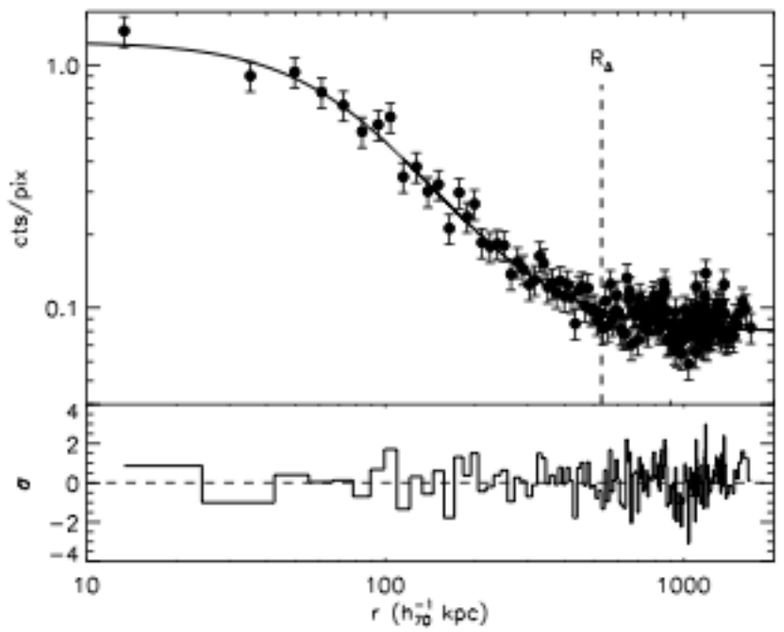

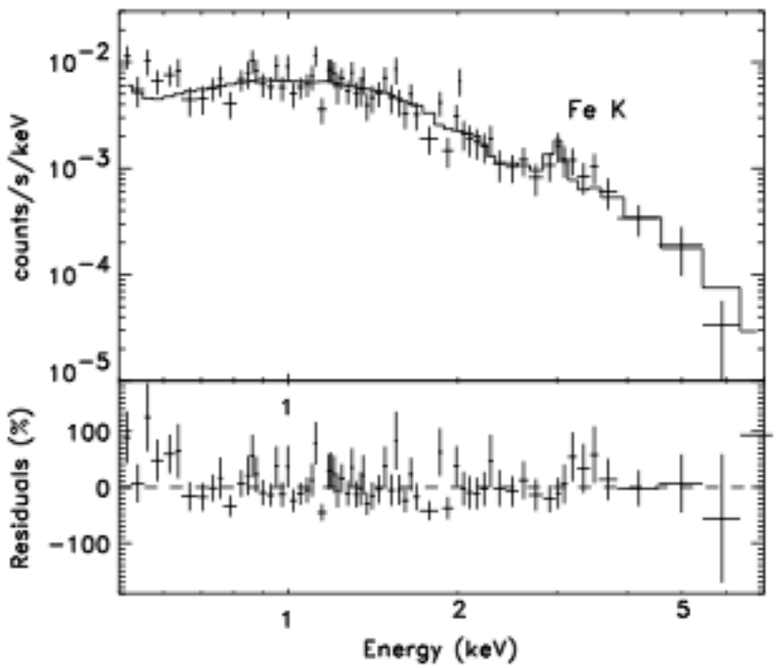

Few photons: luminosity bias

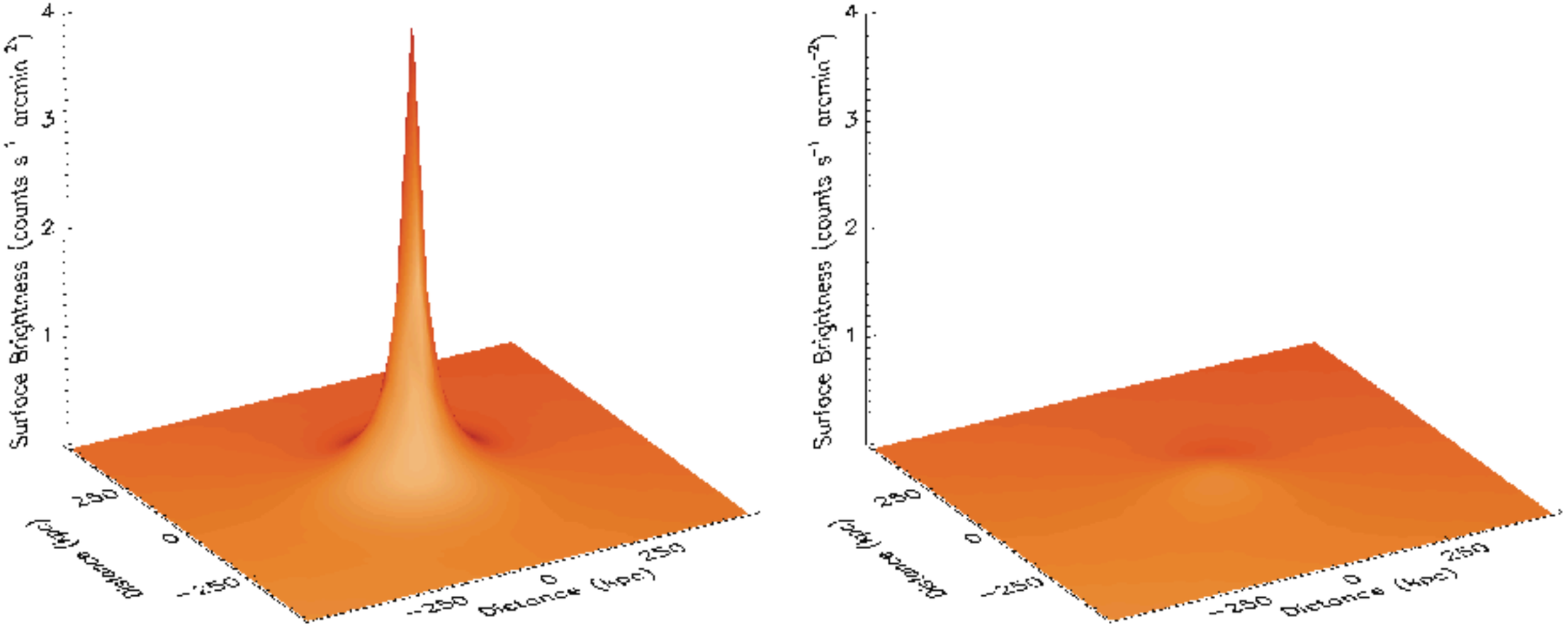

Figure 7. The three-dimensional representation of the projected surface brightness for the cool-core cluster Abell 2029 (left-hand panel) and the radio halo cluster Abell 2319 (right-hand panel) scaled to appear as they would if observed at the same redshift. The flat surface brightness core of Abell 2319 with respect to that of Abell 2029 (core radius of 120 versus 20 kpc, respectively) is the most obvious morphological distinction and impacts on the relative importance of projection effects in the two systems. The *X*- and *Y*-axes span 1 Mpc on a side. The *Z*-axis shows the surface brightness in units of counts s^{-1} $arcmin^{-2}$.

From Million & Allen (2009)

Few photons: luminosity bias

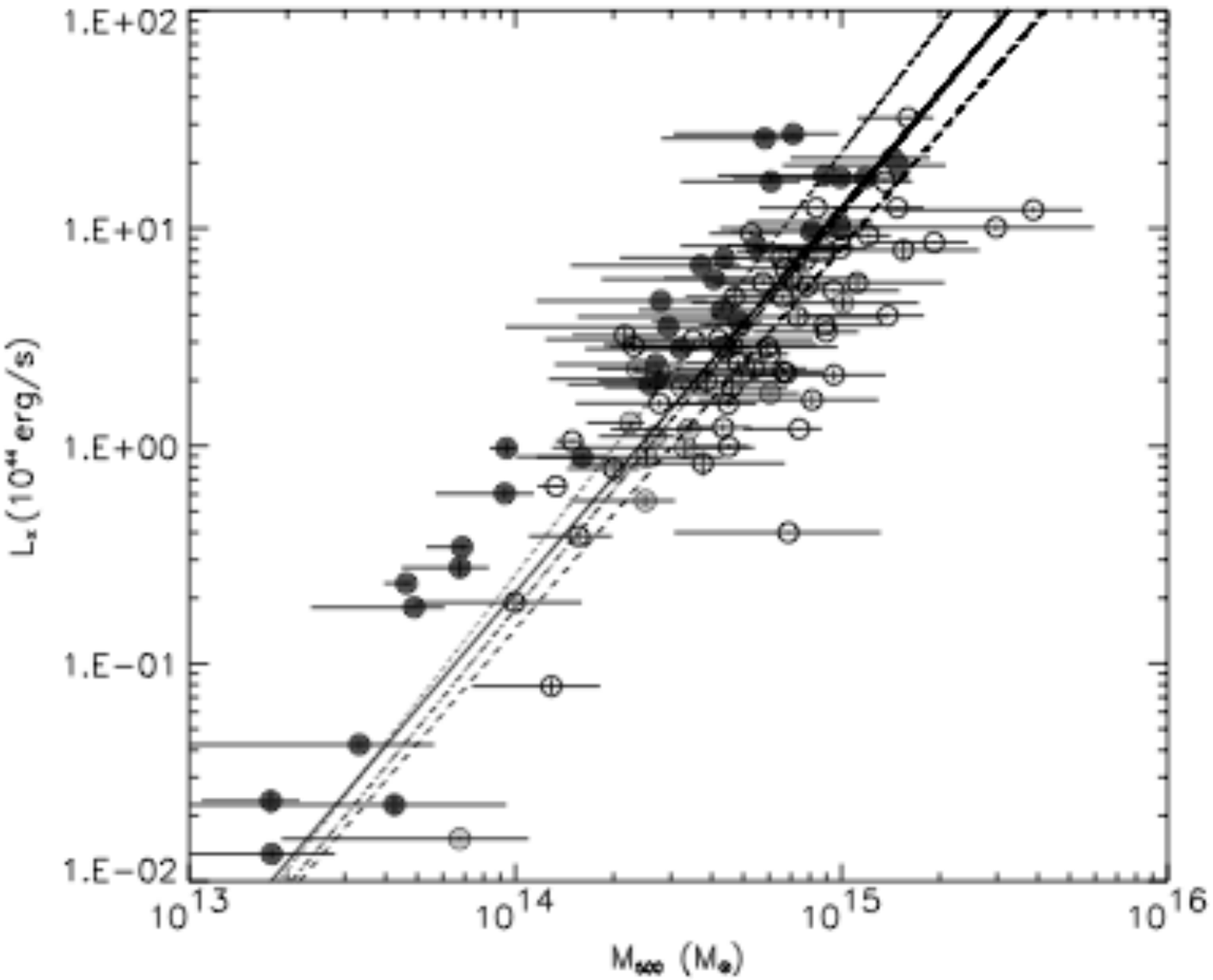

Chen, Reiprich, Boehringer, Ikebe, Zhang (2007)

Y_X: a low-scatter mass proxy

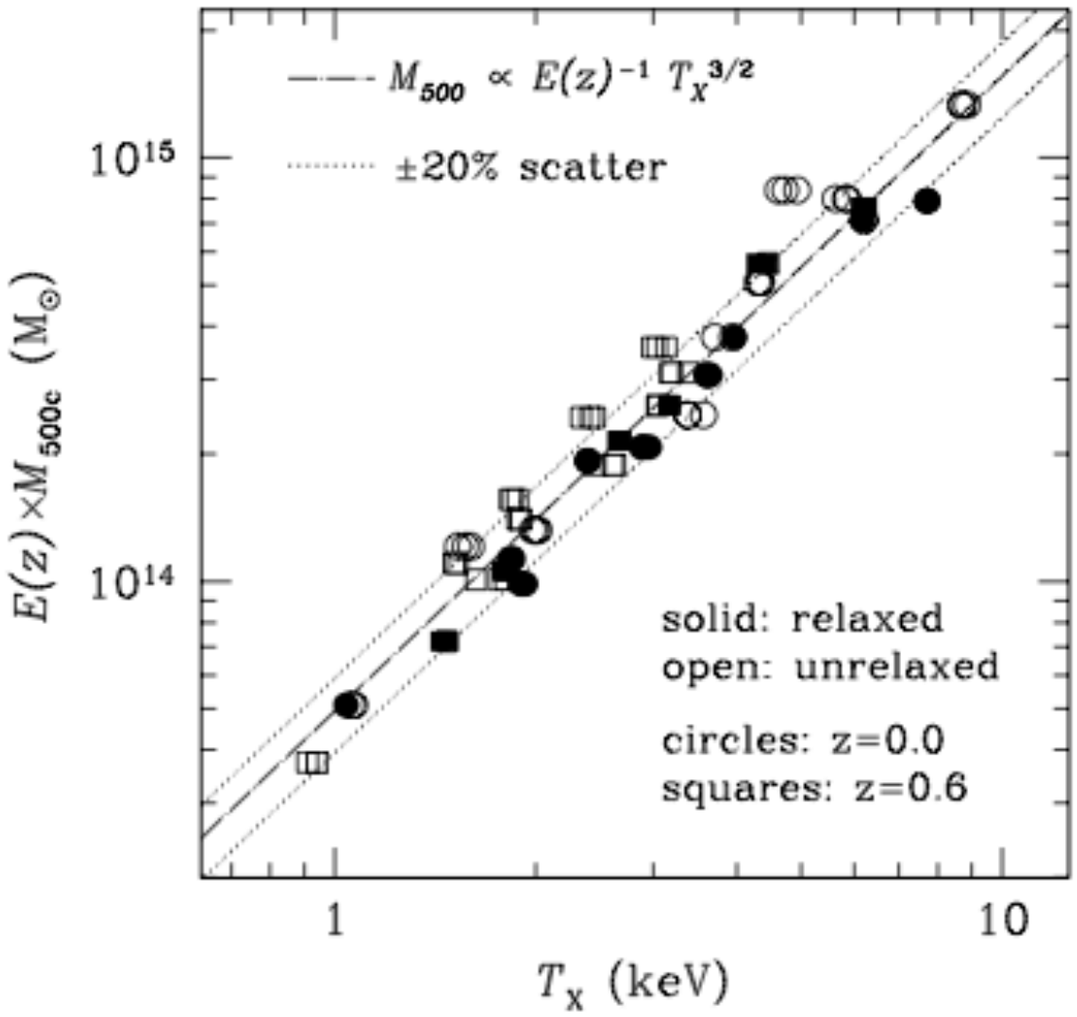

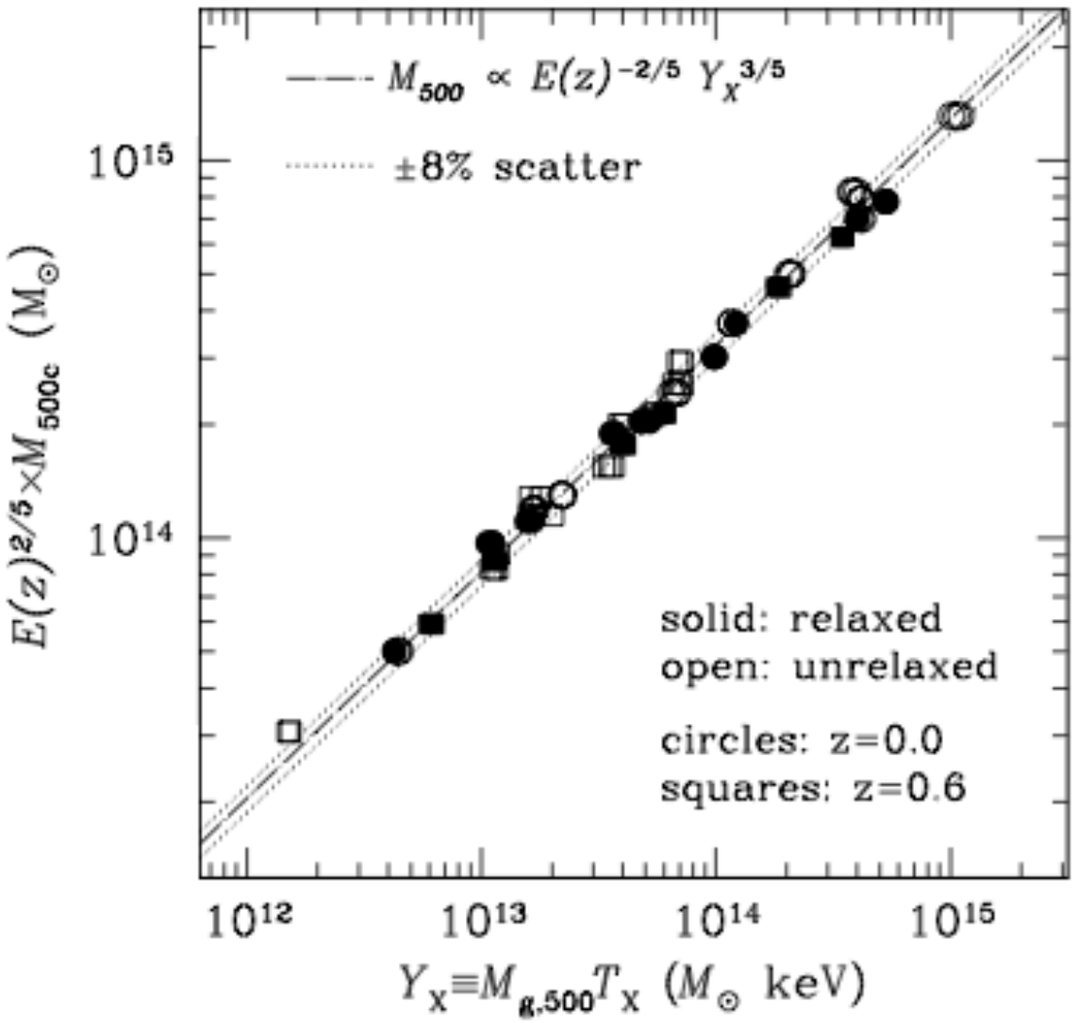

M_{gas} is also good mass proxy, but relatively larger scatter (~15%)

Figure from Kravtsov, Vikhlinin & Nagai (2006)

Y_X: a low-scatter mass proxy

$$Y_{\rm X} \equiv M_{g,500} T_{\rm X}$$

Yx is defined analogous to SZ integrated Y parameter: it is the X-ray analogue of total thermal pressure

decrement in Rayleigh-Jeans part: $\Delta I(\nu) = -2\, y\, I(\nu)$

Compton-y parameter: $y \equiv \frac{\sigma_{\rm T}\, k_{\rm B}}{m_{\rm e}\, c^2} \int T_{\rm e}\, n_{\rm e}\, dl$

integrated effect: $Y = \int y\, dA \propto n_{\rm e}\, T\, dV \propto E_{\rm thermal}$

Y_x and Y_{sz} comparison

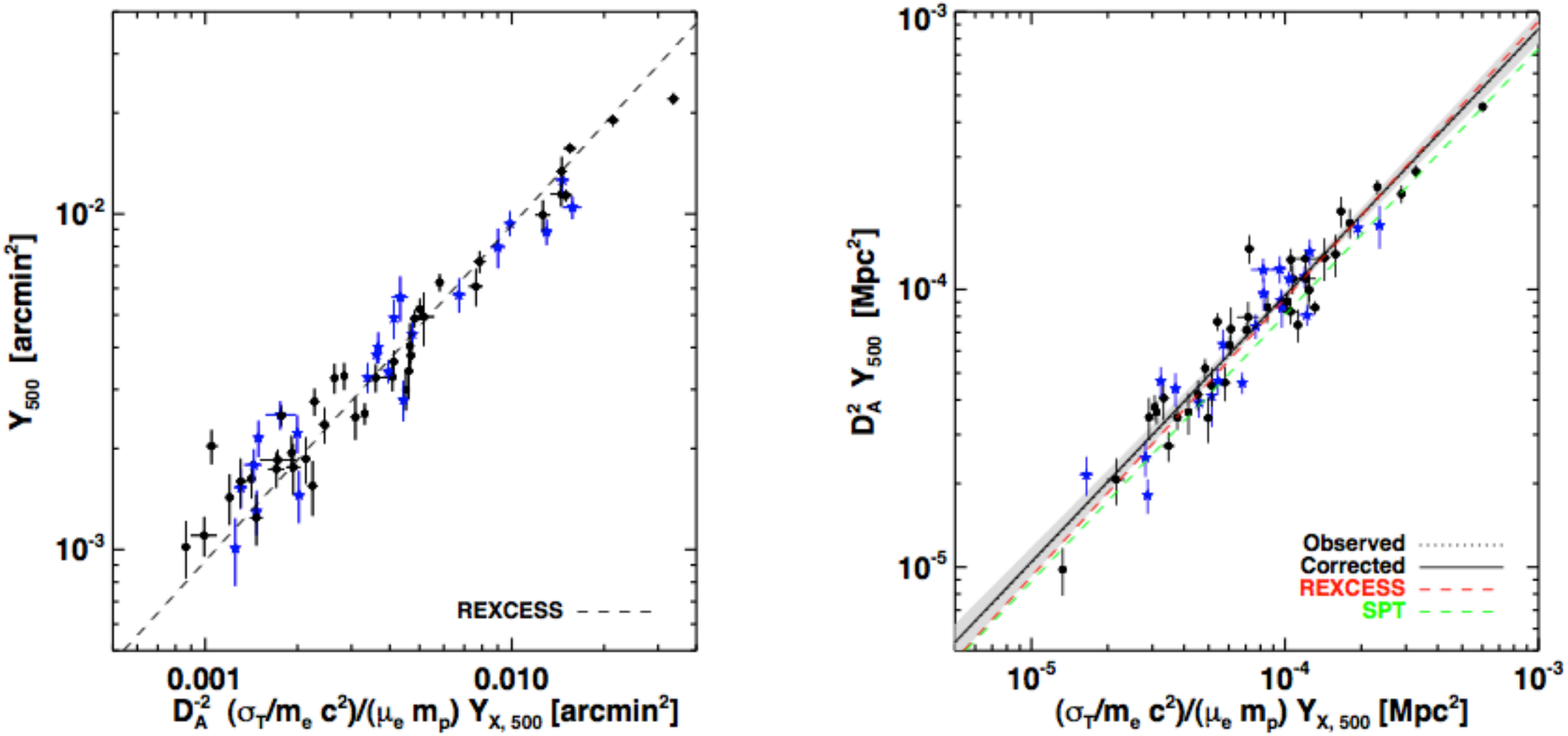

Fig. 4: SZ flux vs X-ray prediction. Blue stars indicate cool core systems. *Left panel:* Relation plotted in units of arcmin^2. The dashed line is the prediction from REXCESS X-ray observations (Arnaud et al. 2010). *Right panel:* Relation plotted in units of Mpc^2. The *SPT* results are taken from Andersson et al. (2010).

From Planck collaboration (2011)

Joint SZ/X-ray modeling

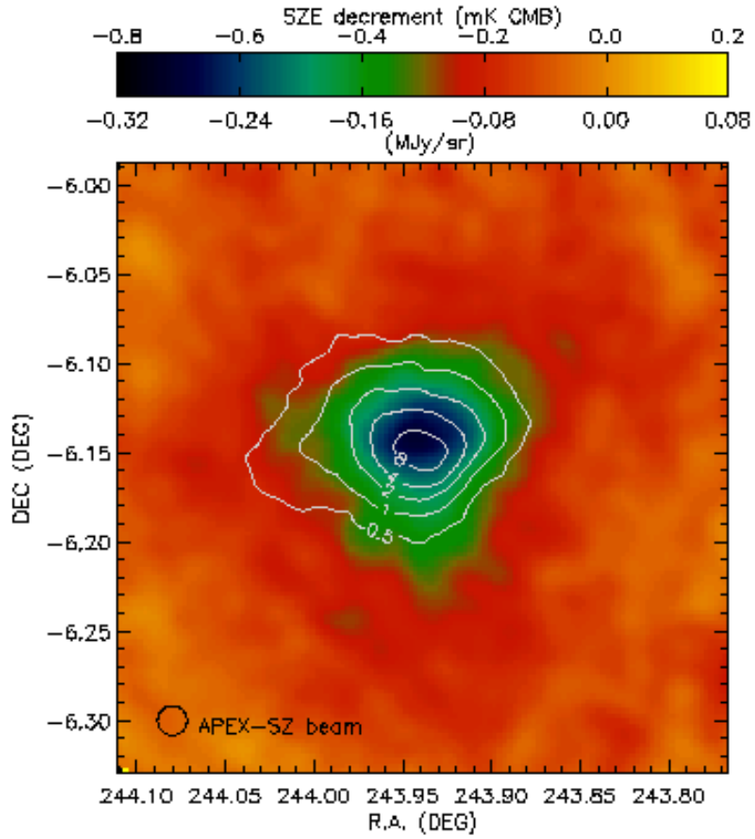

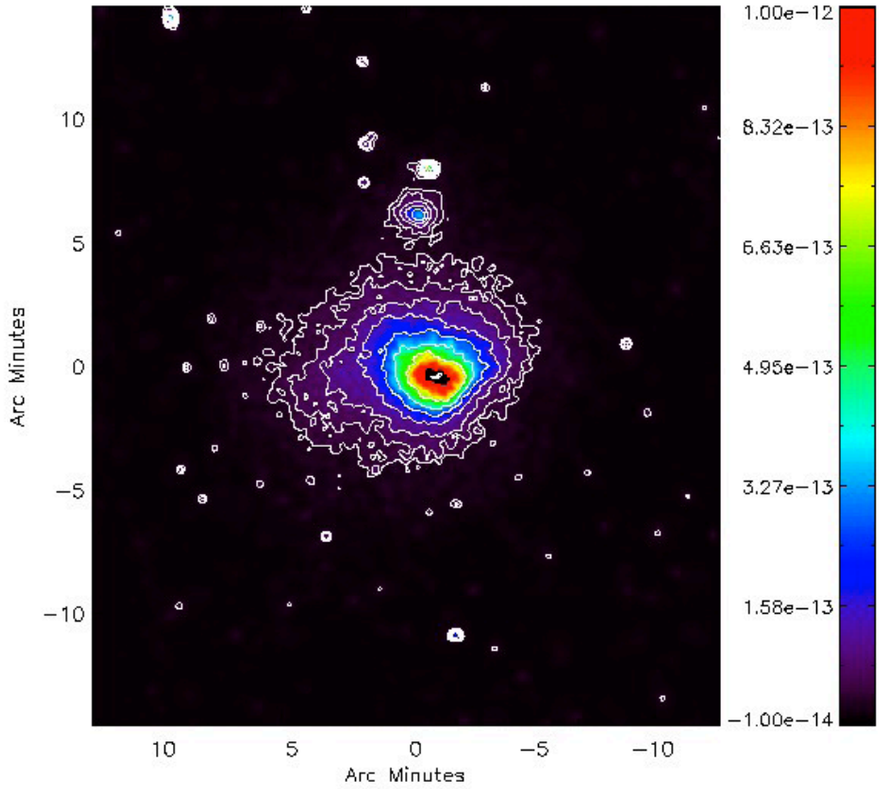

$$\Delta T(R) \propto 2\int_R^\infty n_e(r)\, T_e(r)\, \frac{r\,dr}{\sqrt{r^2-R^2}}$$

$$S_X(R) \propto 2\int_R^\infty n_e^2(r)\, T_e(r)^{1/2}\, \frac{r\,dr}{\sqrt{r^2-R^2}}$$

$$f(\theta) = \int_{-\infty}^{\infty} g(r)dl = 2\int_{d_A\theta}^{\infty} g(r)\,\frac{rdr}{\sqrt{r^2-d_A^2\,\theta^2}}\,, \quad \Rightarrow \quad g(r) = \frac{1}{\pi d_A}\int_{\infty}^{r/d_A}\frac{df(\theta)}{d\theta}\,\frac{d\theta}{\sqrt{\theta^2-r^2/d_A^2}}\,.$$

Abel Inversion

The Abel transform of a function f(r) is given by

$$F(y) = 2\int_y^\infty \frac{f(r) r\, dr}{\sqrt{r^2 - y^2}}.$$

Assuming f(r) drops to zero more quickly than 1/r, the inverse Abel transform is given by

$$f(r) = -\frac{1}{\pi}\int_r^\infty \frac{dF}{dy}\frac{dy}{\sqrt{y^2 - r^2}}.$$

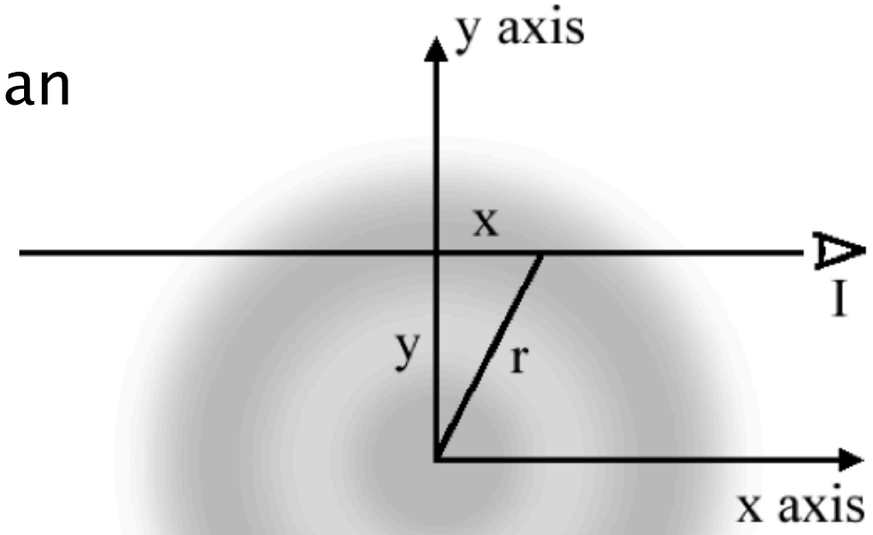

Density and temperature profiles

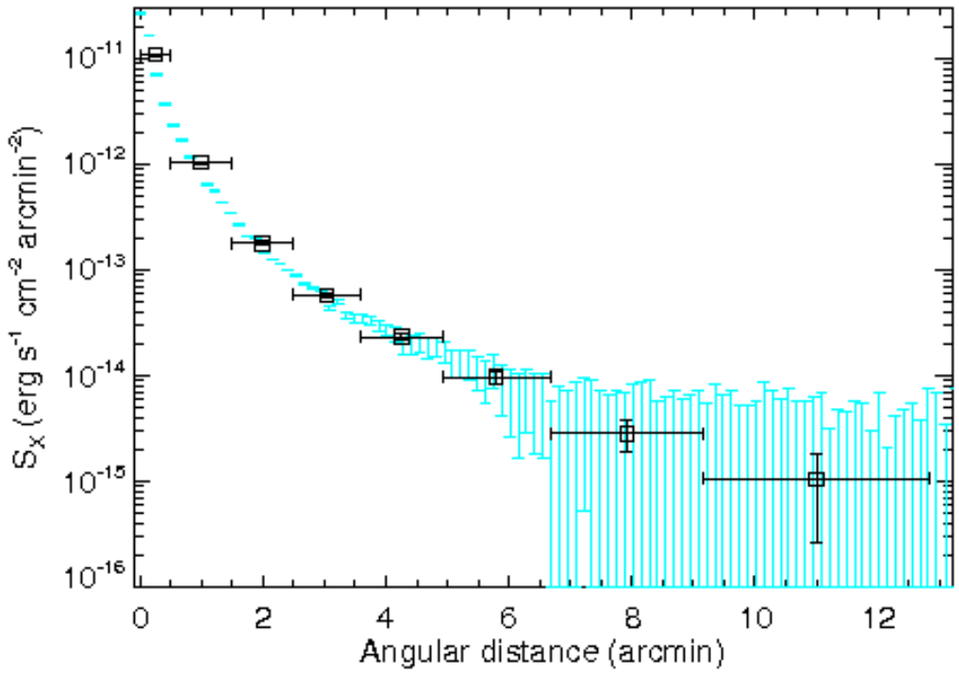

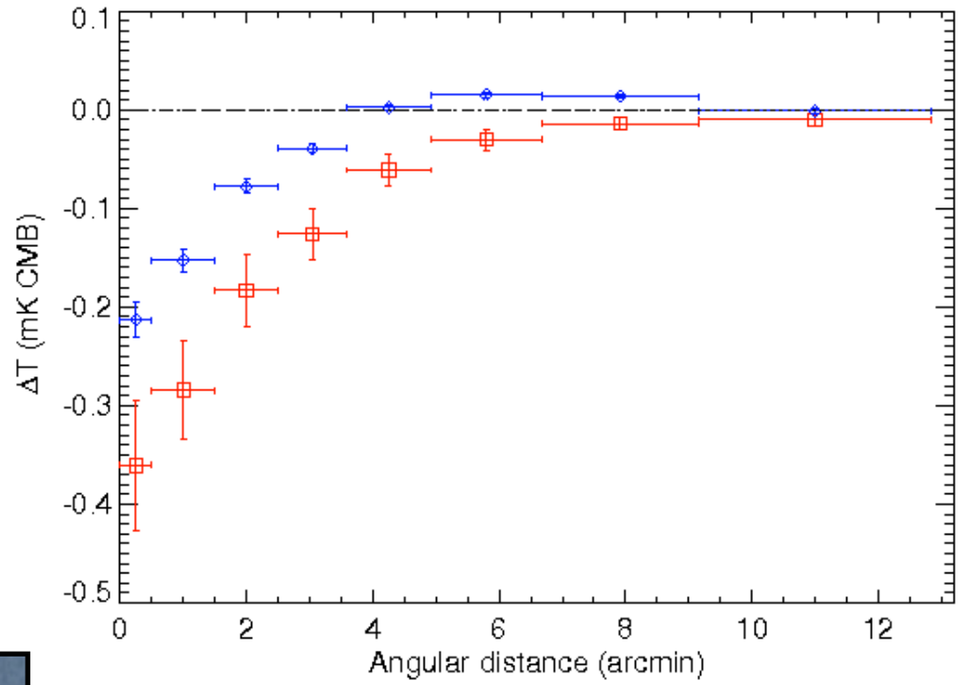

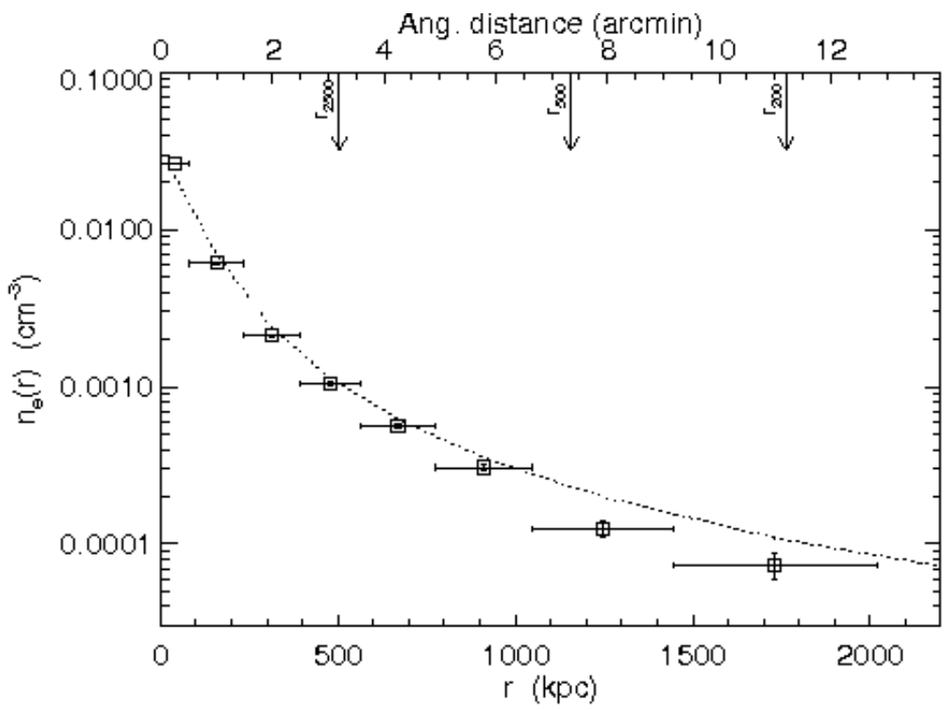

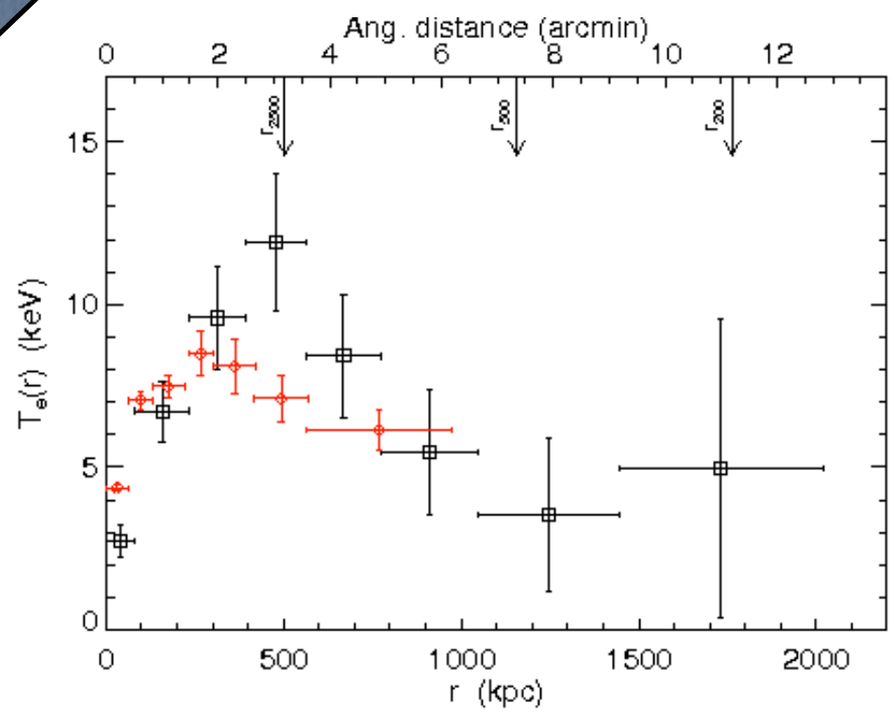

SZ/X-ray Abel inversion results

Abell 2204 mass

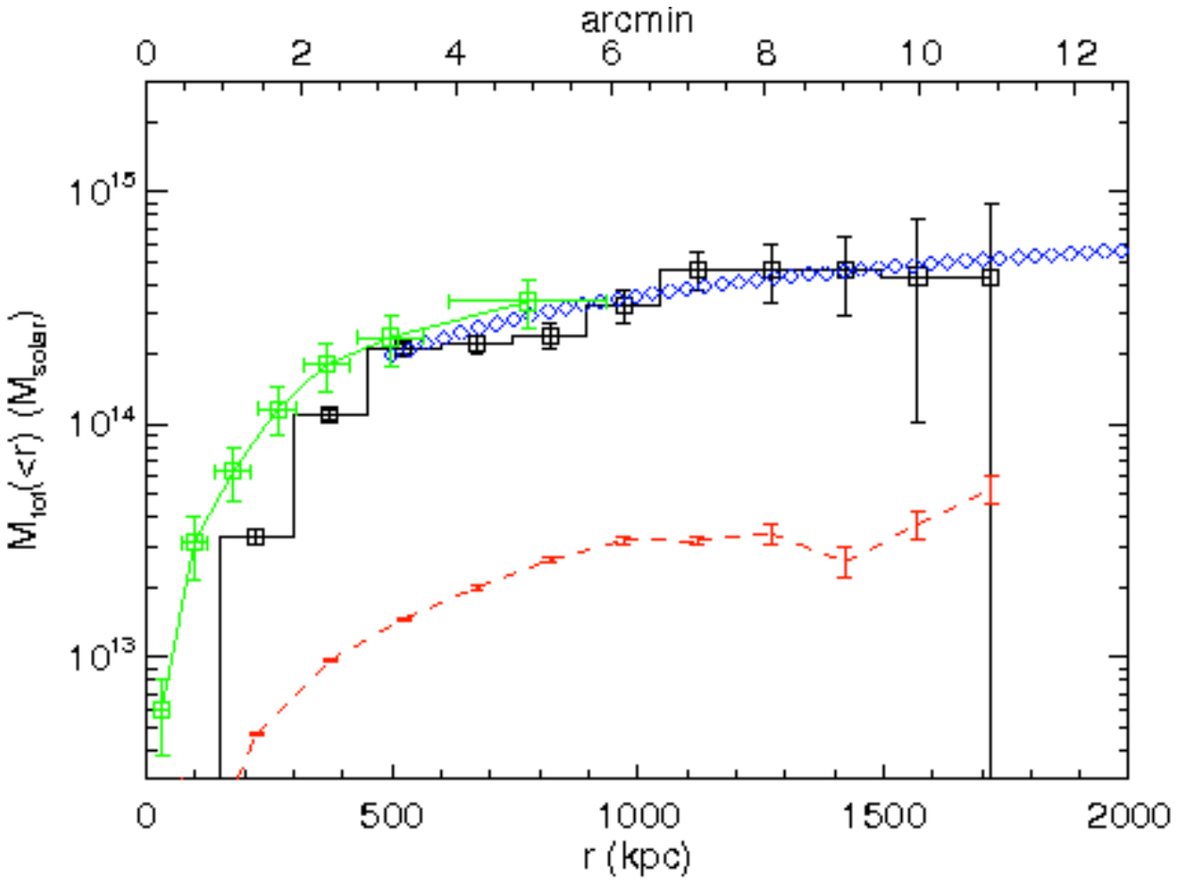

Entropy profile comparison

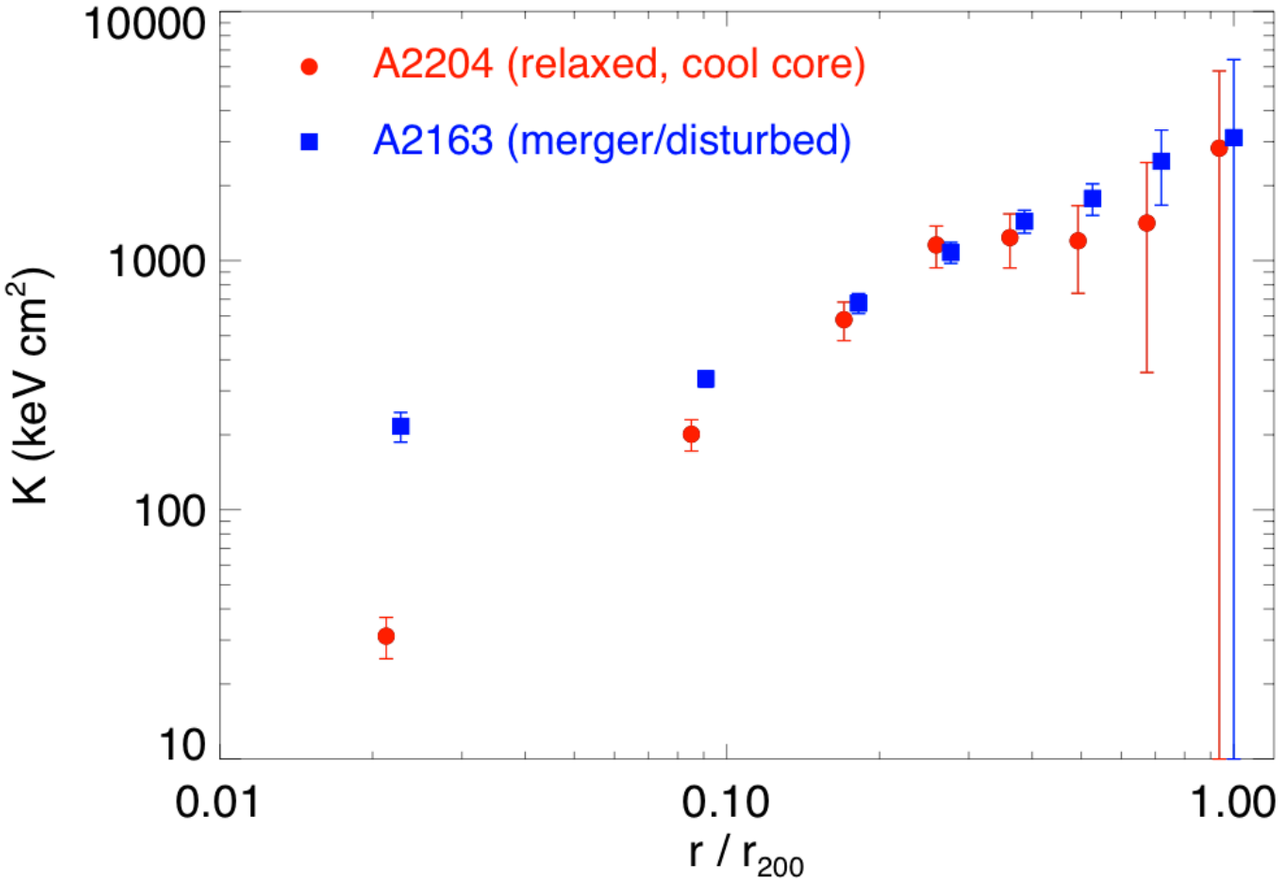

High-resolution SZ

MACS0744

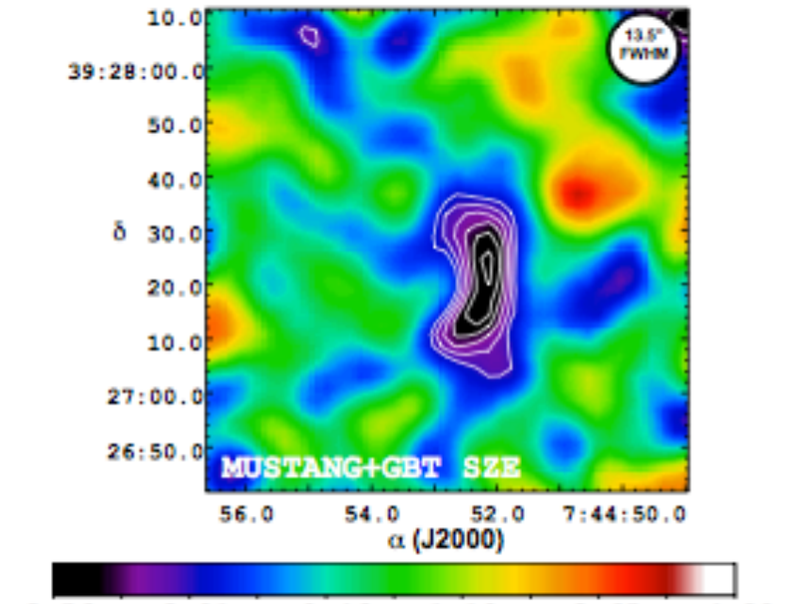

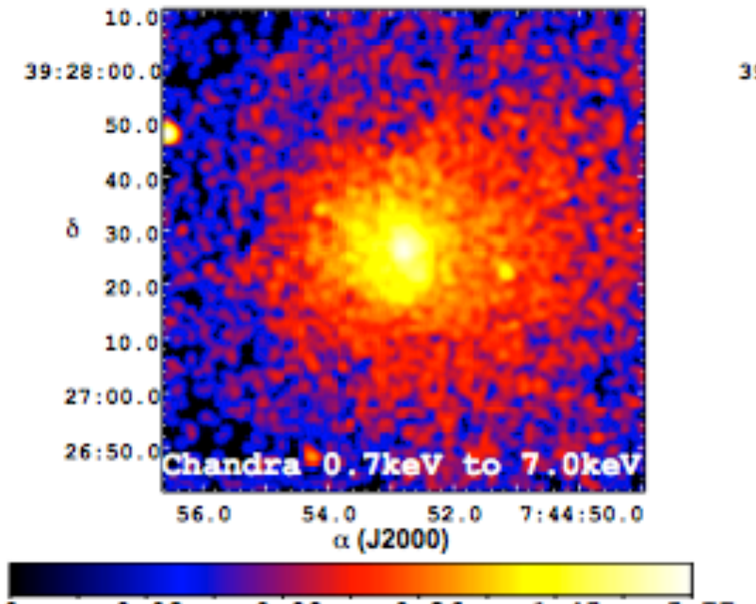

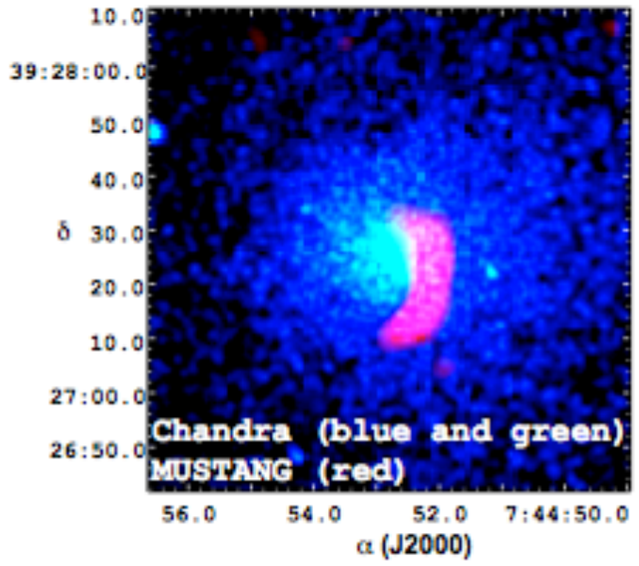

Korngut et al. 2010

A1835

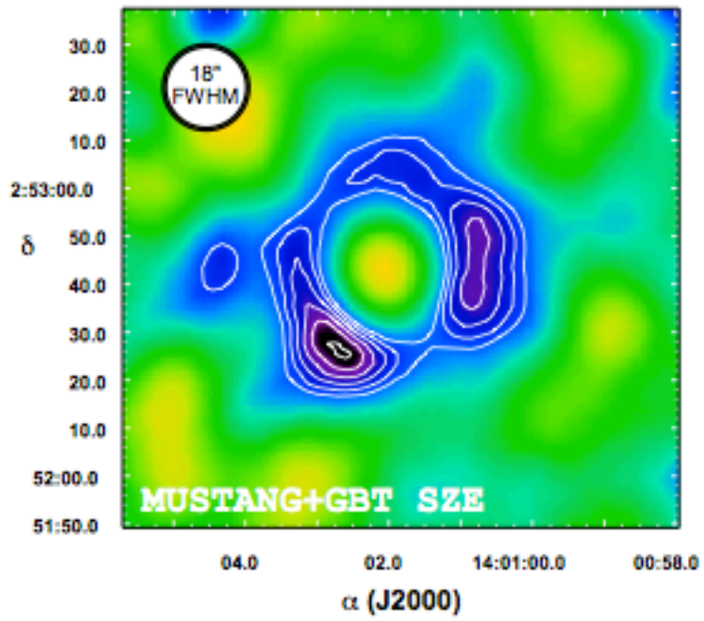

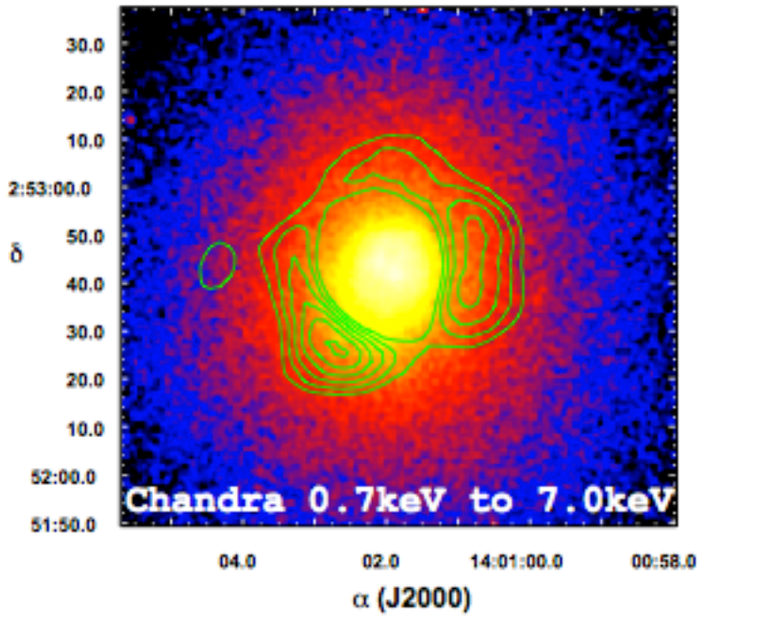

Mergers, shocks and bubbles

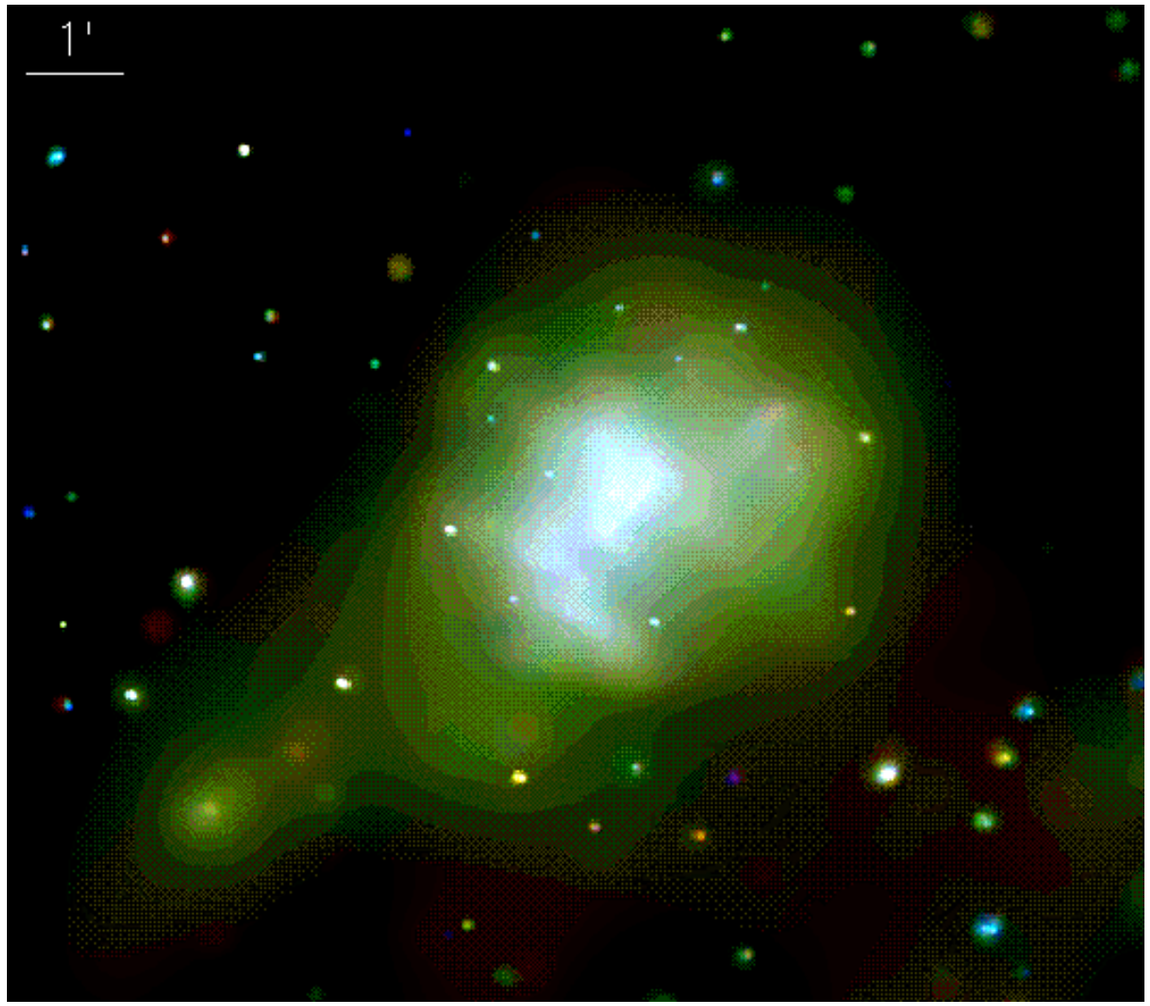

J0717.5+3745 at z = 0.548

Clearly disturbed, shock-like substructure, filament. What will SZ image look like?

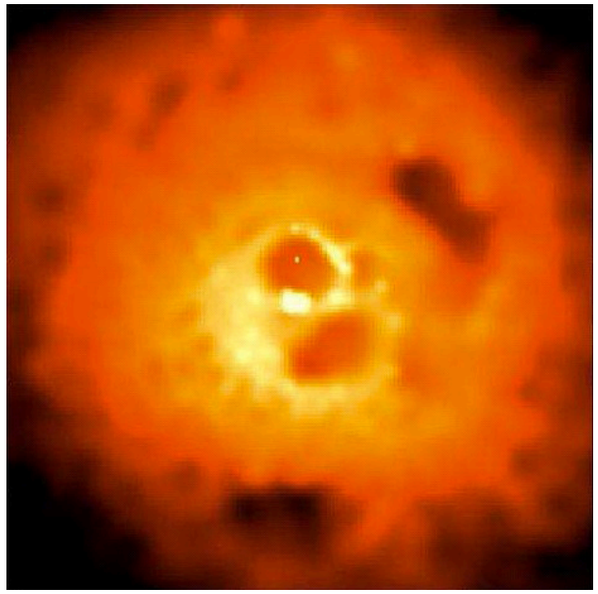

Perseus cluster

Abell 2052

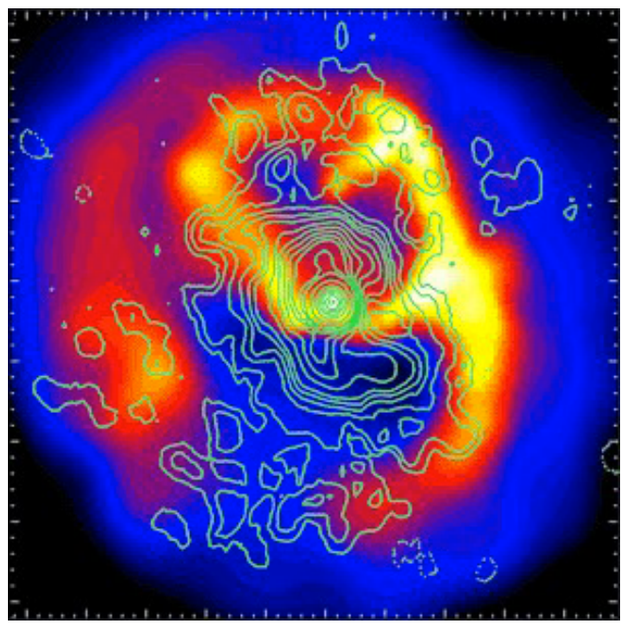

Future: SZ imaging with ALMA

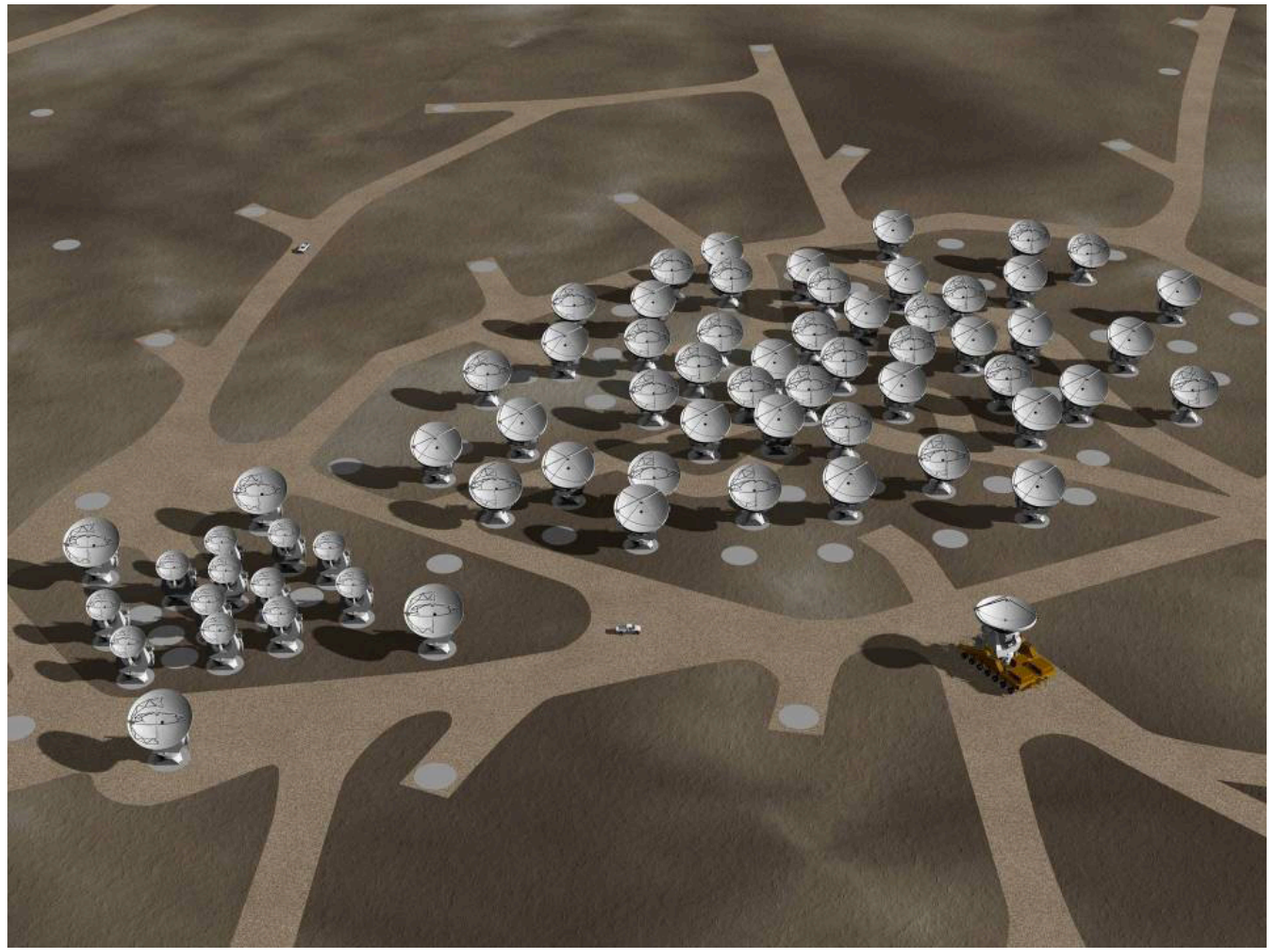

ν (GHz)	λ/D (arcsec)					
	Primary beam		Shortest spacing		Resolution	
	12m array *(compact)*	ACA	12m array	ACA	12m array	ACA
35	170	291	116	199	10	60
110	56	99	37	64	3.1	19

Future: SZ imaging with CCAT

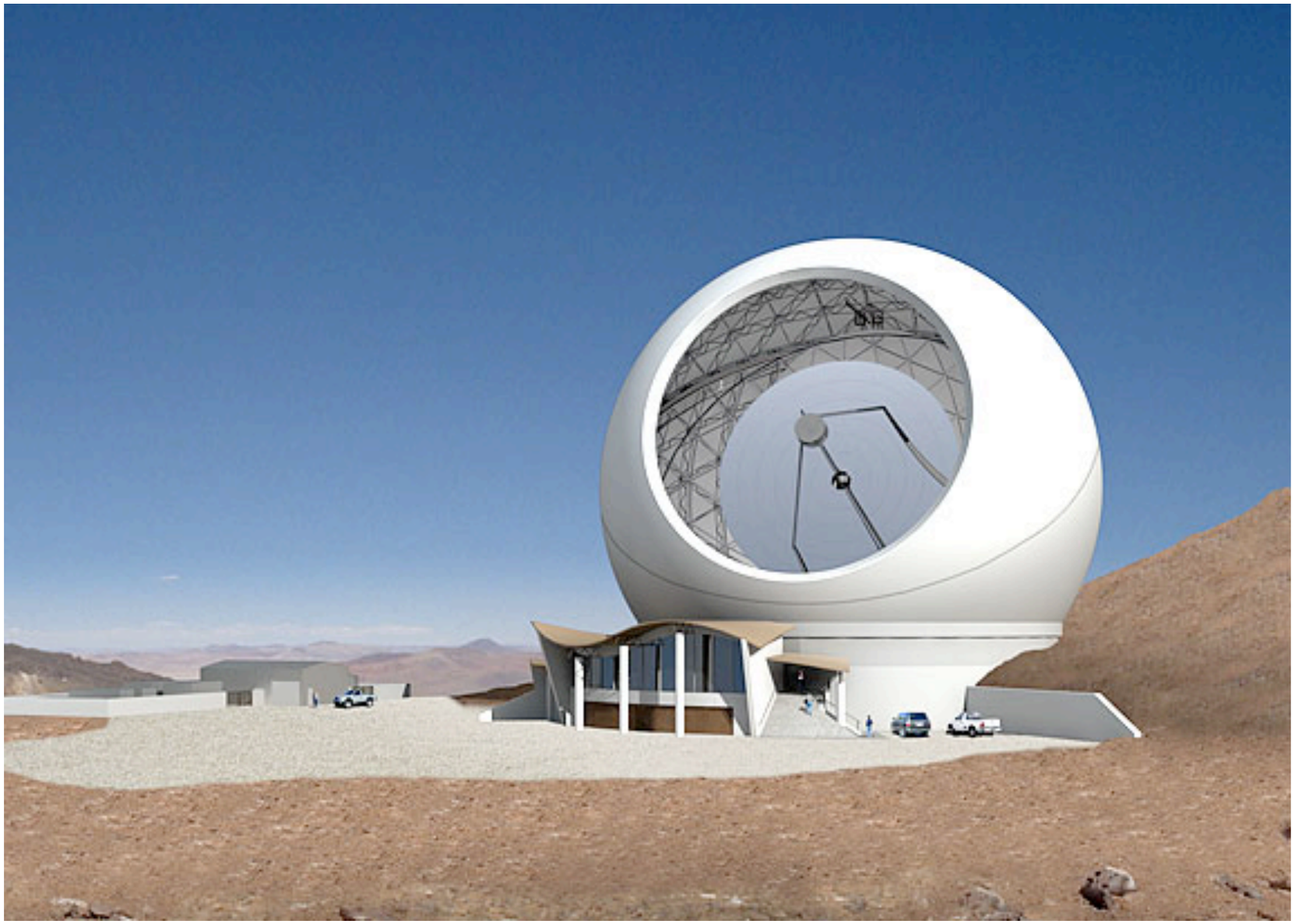

Partners: Cornell, Caltech, Assoc. Univ. (US),
McGill, Toronto (Canada), **Bonn, Cologne (Germany)**

SZ power spectrum

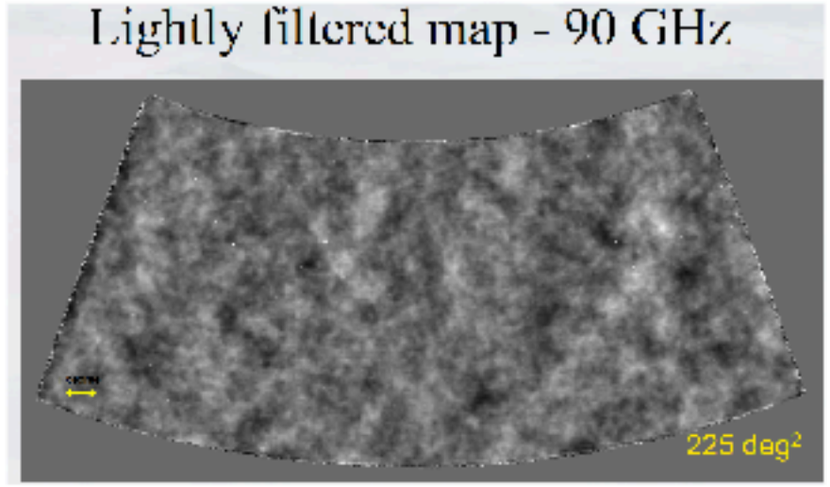

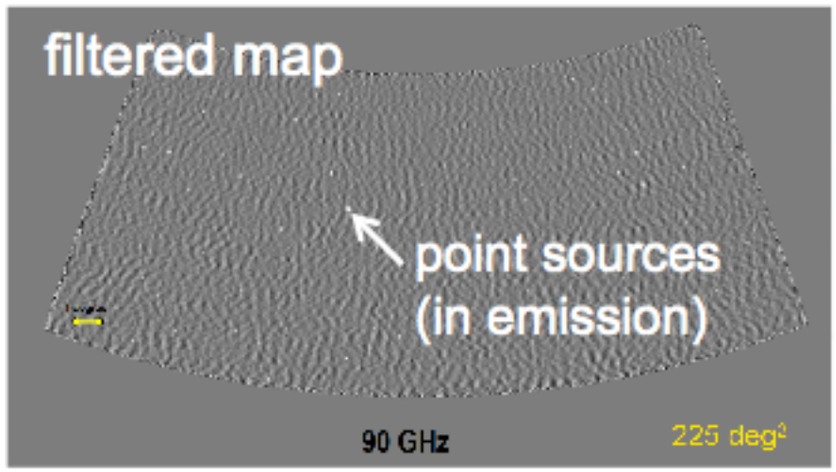

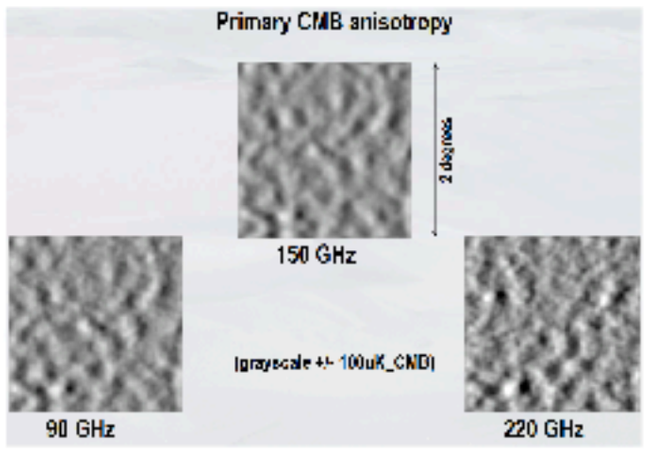

Cluster Finding in Real SPT Observations

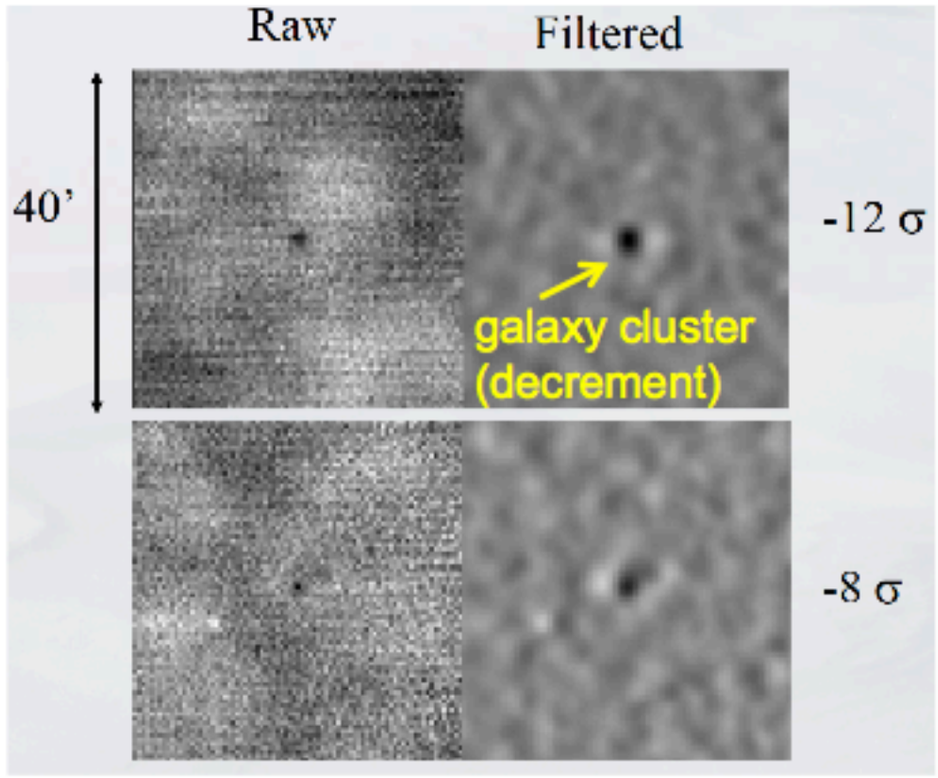

Source: http://member.ipmu.jp/clj2010//program_files/Talks/holzapfel.pdf

SZ power spectrum

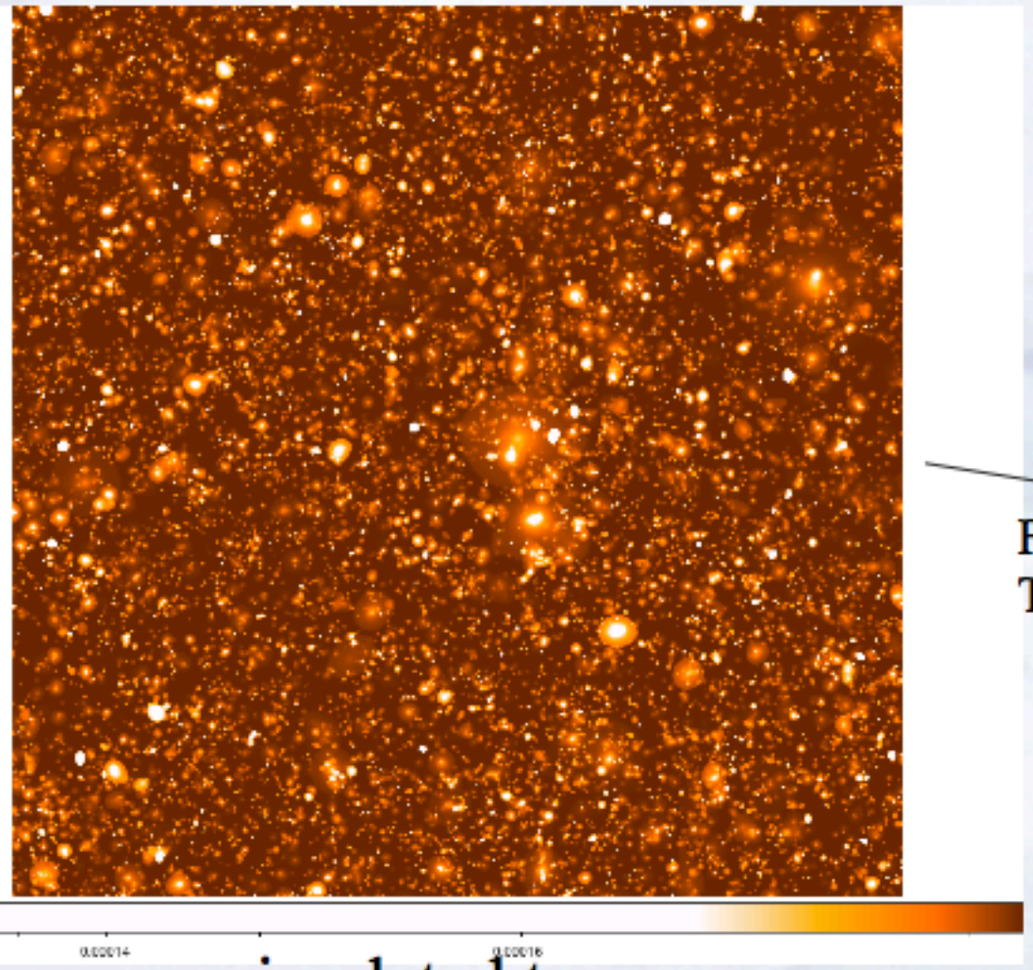

simulated tsz map

10deg

Fourier Transform

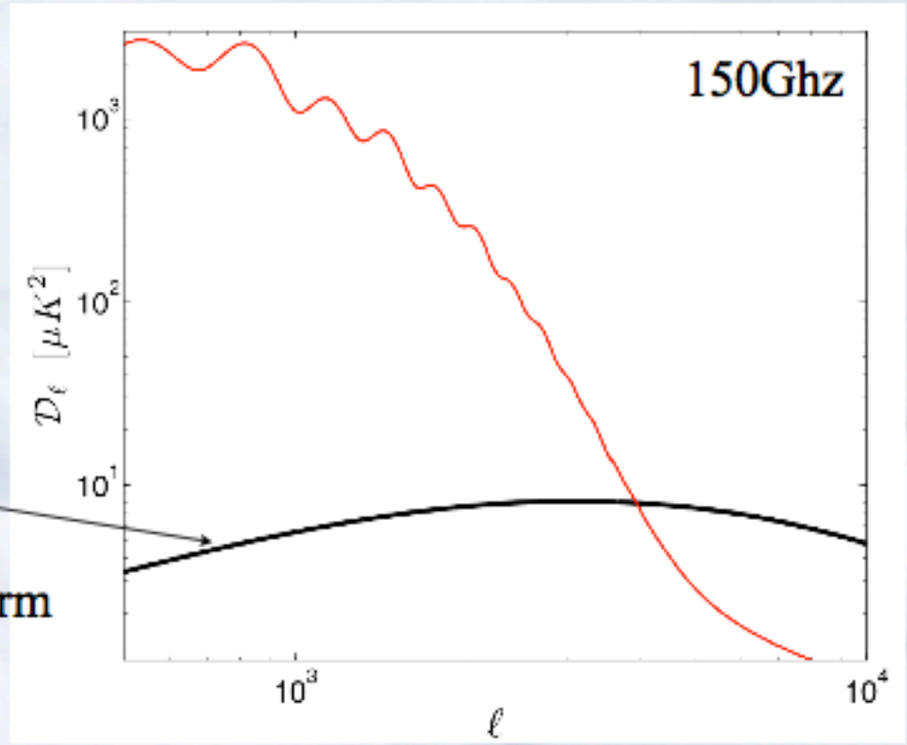

$(D_l = l\,(l+1)\,c_l\,/\,2\,\pi)$

16

Simulations from Shaw et al. (09); Sehgal et al. (10)

SZ power spectrum

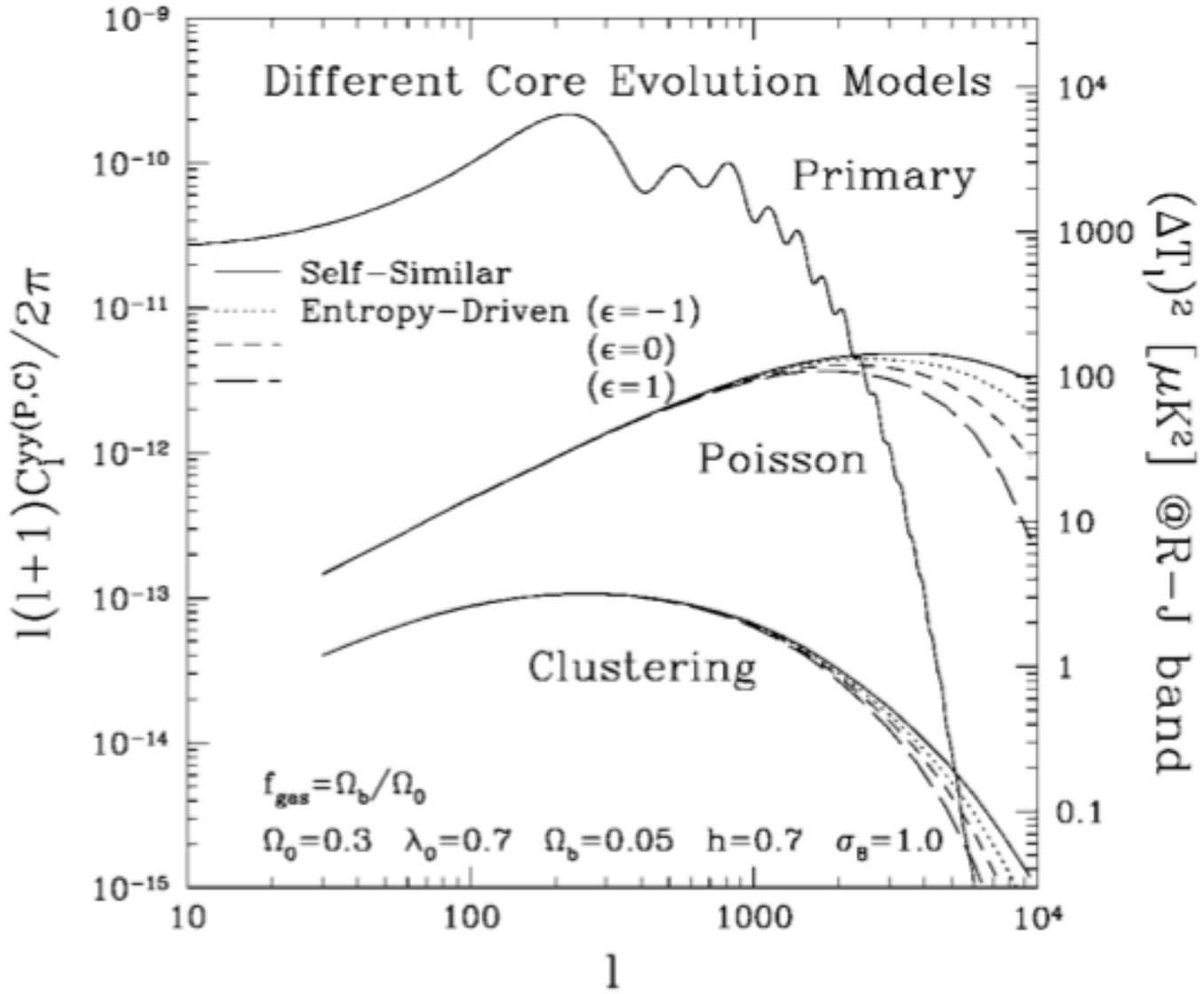

Komatsu & Kitayama 1999

SZ power spectrum

Cosmology

Astrophysics
(electron pressure profile)

$$C_l^{yy(P)} = \int_0^{z_{\rm dec}} dz \frac{dV}{dz} \int_{M_{\rm min}}^{M_{\rm max}} dM \frac{dn(M,z)}{dM} |y_l(M,z)|^2 , \quad (4)$$

$$C_l^{yy(C)} = \int_0^{z_{\rm dec}} dz \frac{dV}{dz} P_m \left(k = \frac{l}{r(z)} , z \right)$$
$$\times \left[\int_{M_{\rm min}}^{M_{\rm max}} dM \frac{dn(M,z)}{dM} b(M,z) y_l(M,z) \right]^2 , \quad (5)$$

Komatsu & Kitayama 1999

SZ power cosmology dependence

Amplitude of SZ power spectrum has sensitive dependence on matter power spectrum normalization

$$C_\ell \propto \sigma_8^{7-9} (\Omega_b h)^2$$

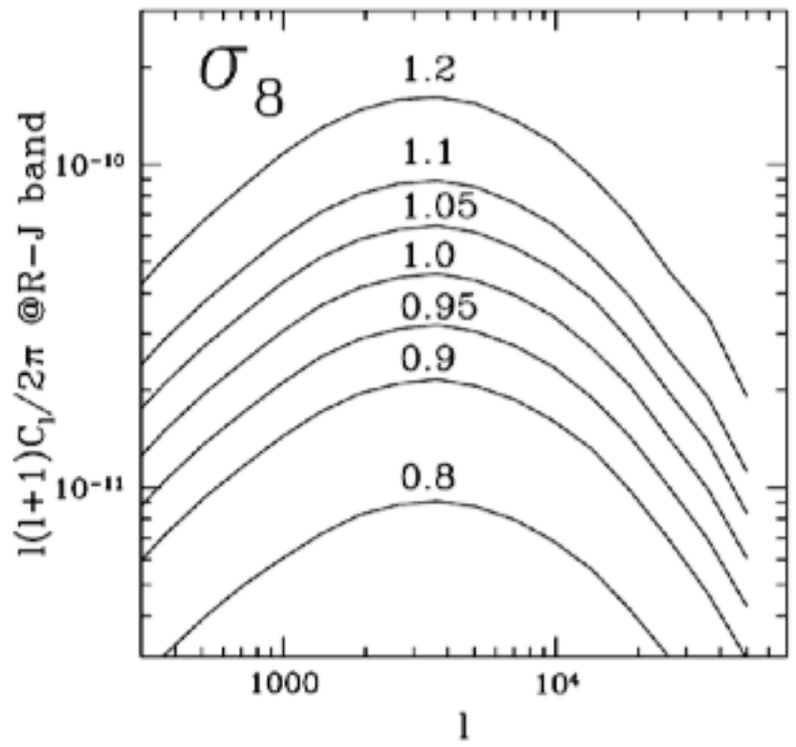

Figure 2. Dependence of the SZ angular power spectrum on σ_8. From top to bottom, the lines indicate $\sigma_8 = 1.2$, 1.1, 1.05, 1.0, 0.95, 0.9, and 0.8, as shown in the figure.

Komatsu & Seljak

SZ power measurement

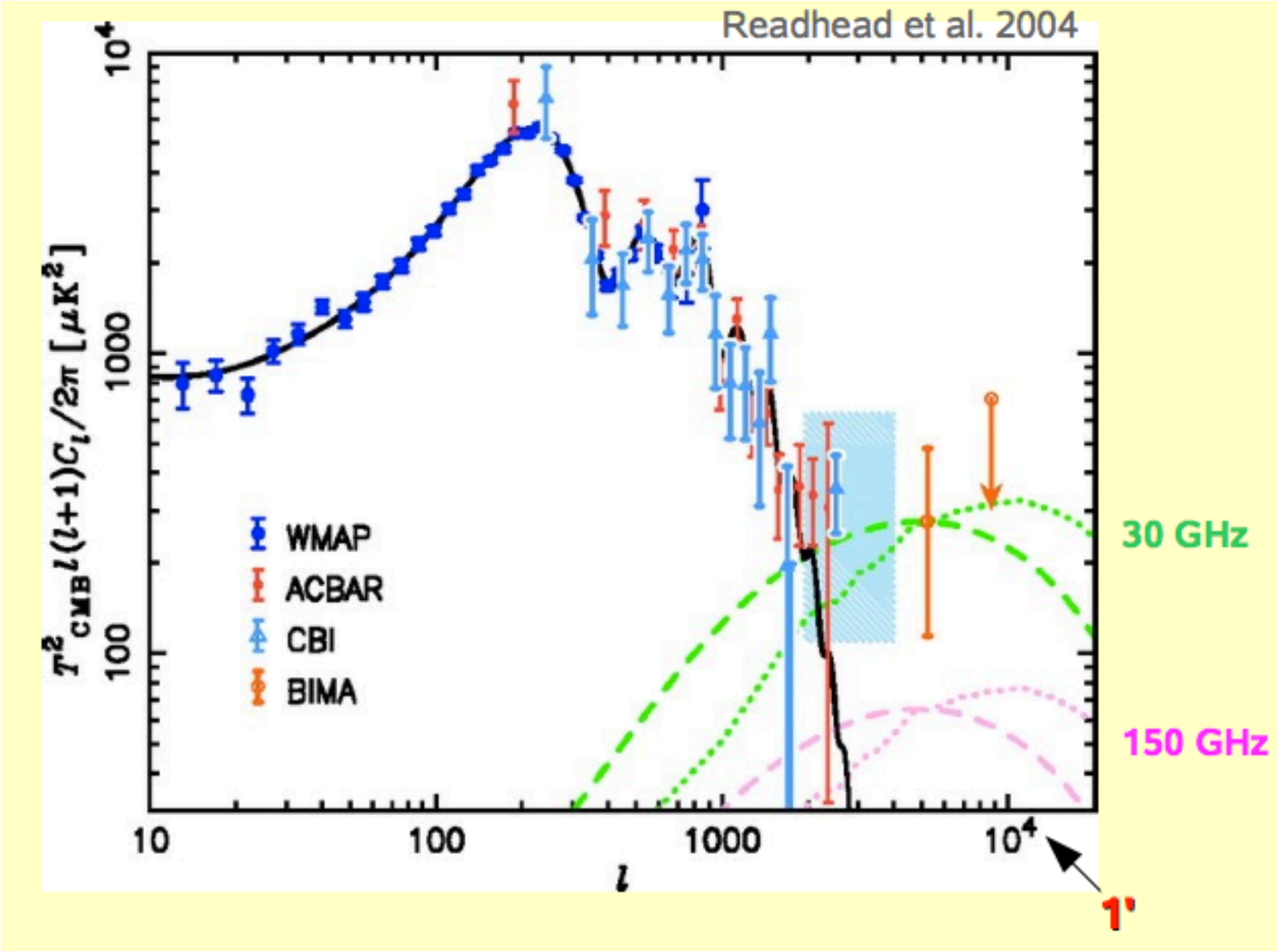

SZ power measurement

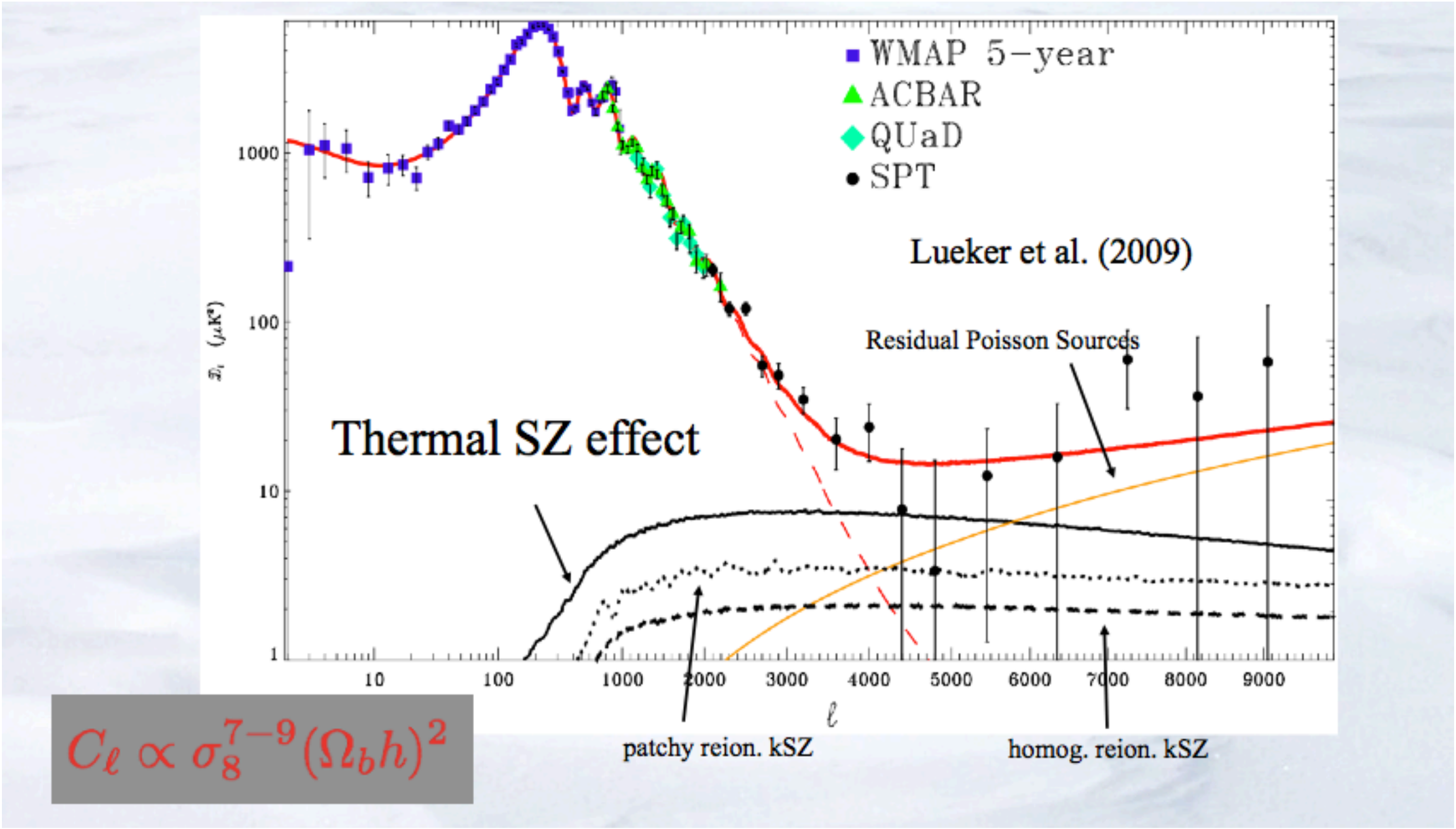

SZ power measurement

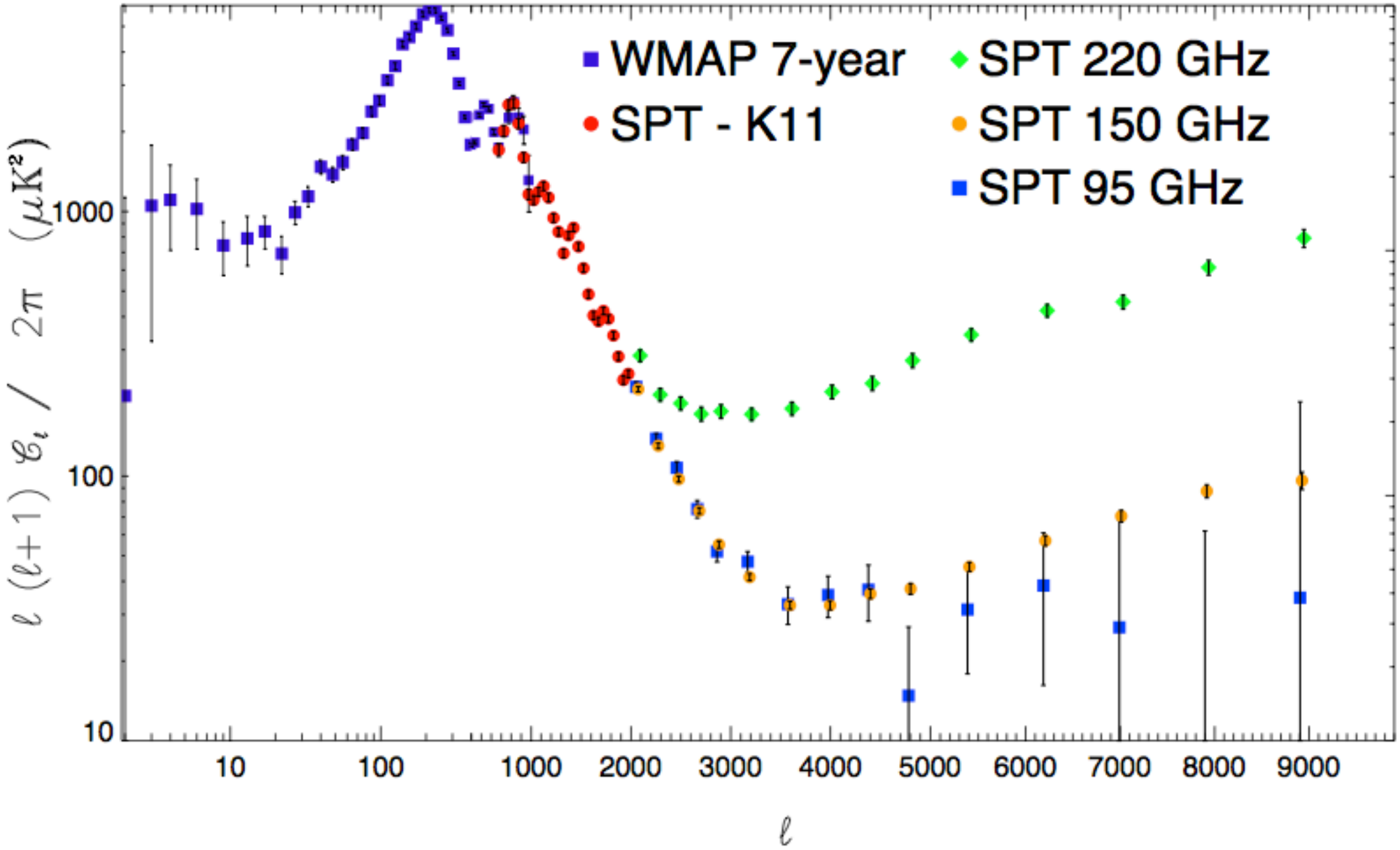

Shirokoff et al. 2011, Reichardt et al. 2012

SZ power measurement

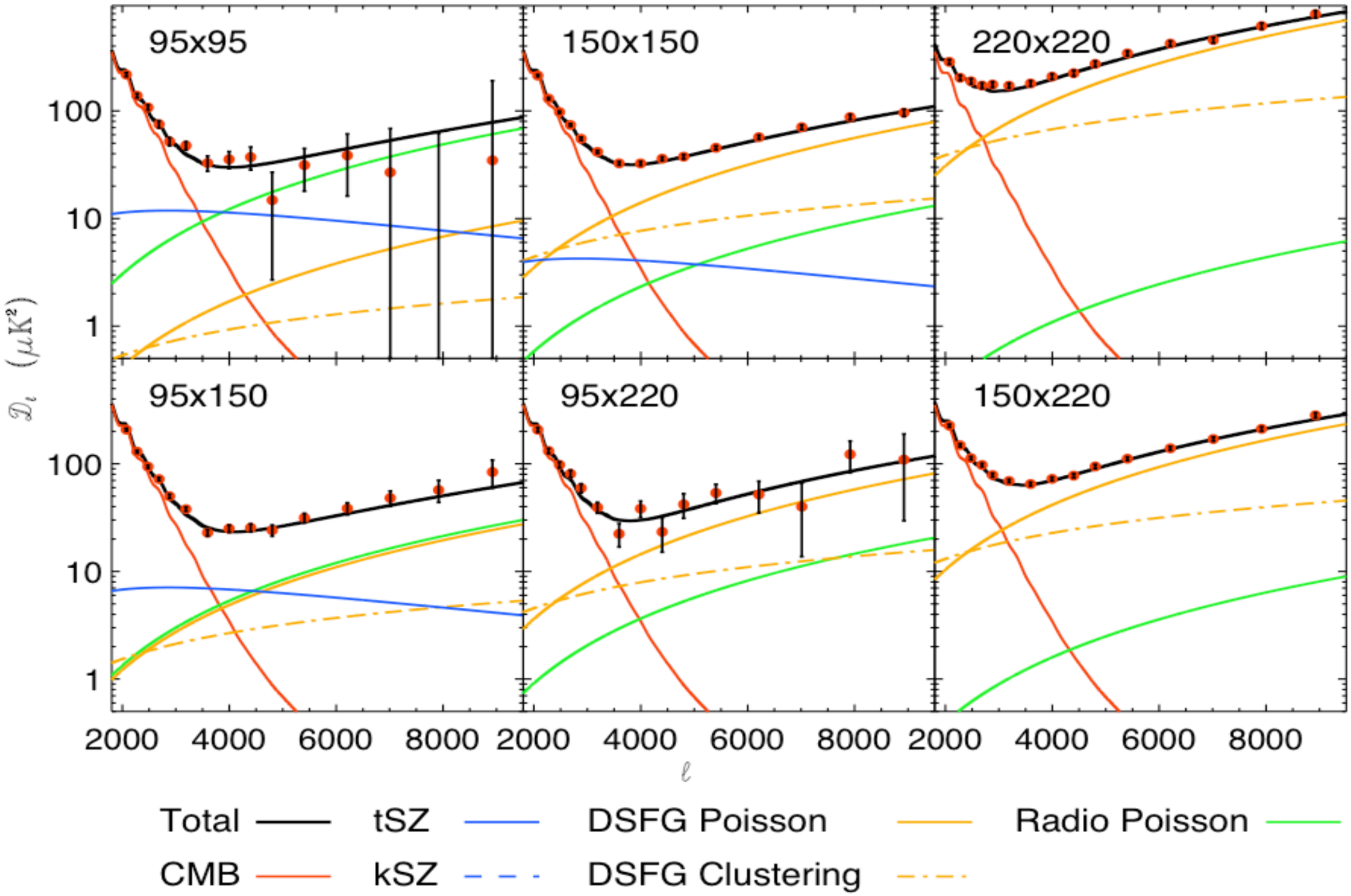

SZ effect "skewness"

ACT data, Wilson et al. 2012

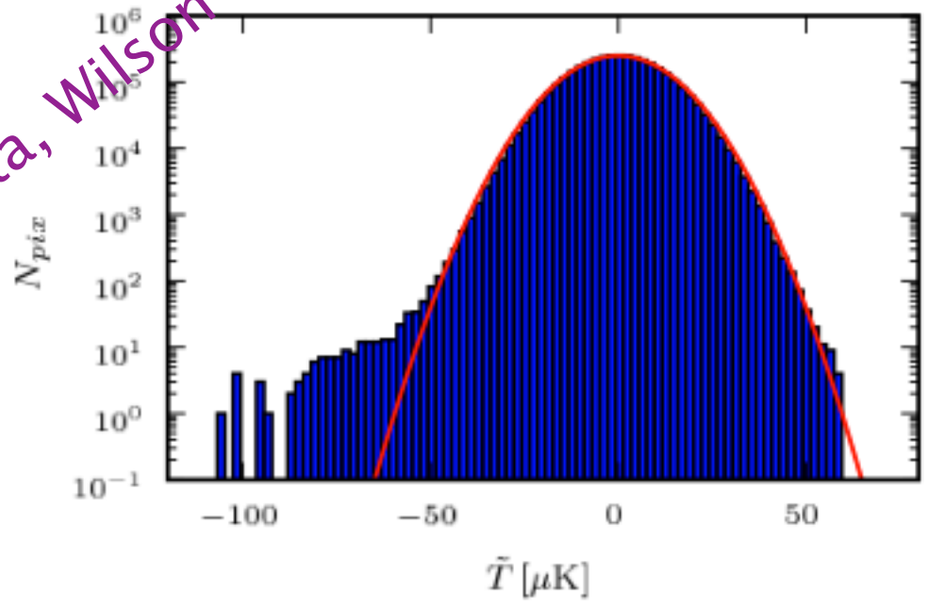

FIG. 2. Histogram of the pixel temperature values in the filtered, masked ACT CMB temperature maps. A Gaussian curve is overlaid in red.

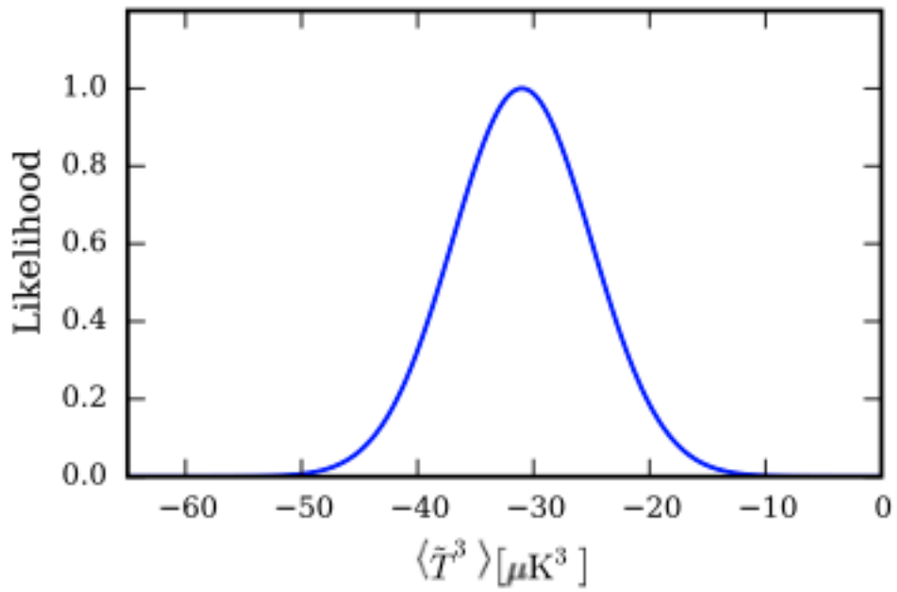

FIG. 3. Likelihood of the skewness measurement described in the text (with measurement errors).

$$\sigma_8^D = \sigma_8^S \left[\frac{\langle \tilde{T}^3 \rangle^D}{\langle \tilde{T}^3 \rangle^S} \right]^{1/\alpha_3}$$

$\alpha_3 \sim 10$!!

Value of σ_8 obtained by comparing with simulations.

$$\sigma_8 = 0.76^{+0.03}_{-0.04}\ (68\%\ \mathrm{C.L.})\ ^{+0.05}_{-0.16}\ (95\%\ \mathrm{C.L.})$$

Massive clusters at high-z

"Pink elephant" clusters

- Several recent detections of > 10^{15} $M_\odot$ clusters at $z > 1$ (x-ray, SZ, ...)

- Are these clusters consistent with the standard cosmological model (including allowed variations of the model parameters)?

- If not, what extensions of the standard model can explain these clusters?

(Slide from Michael Mortonson)

Massive clusters at high-z

Increasing Volume versus Decreasing Number Density

$V_{com}(<z)$ & dV/dz

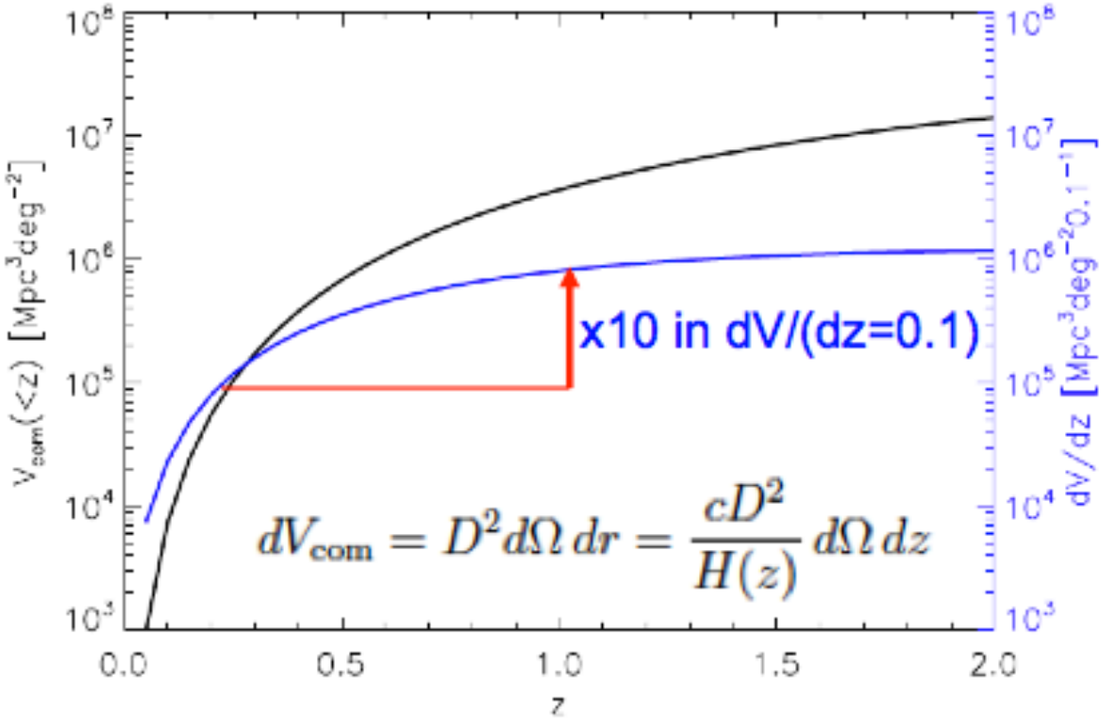

comoving volume
per redshift shell dz=0.1 at z≥1:
~10^6 Mpc^3 deg^{-2}

$n(M_{cl}>5x10^{14}M_{sun})$ / Mpc^3

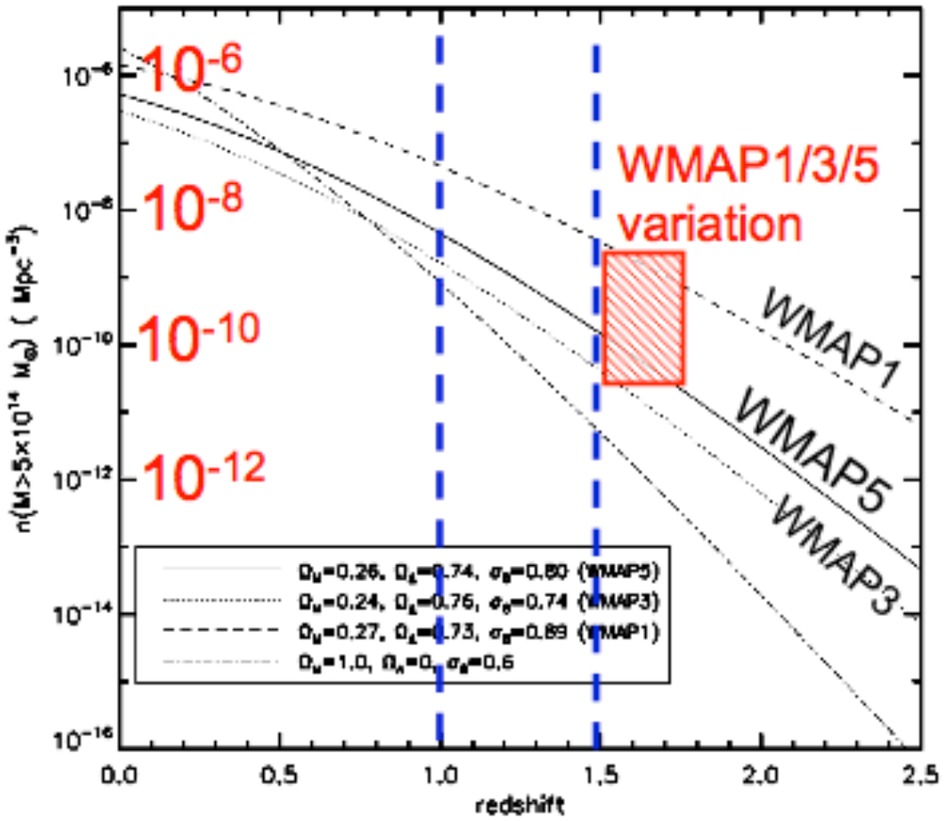

number density of massive
clusters drops by a factor of
100 from z=0→1
3000 from z=0→1.5

Source: Jee et al. 2009

Searching for high-z clusters

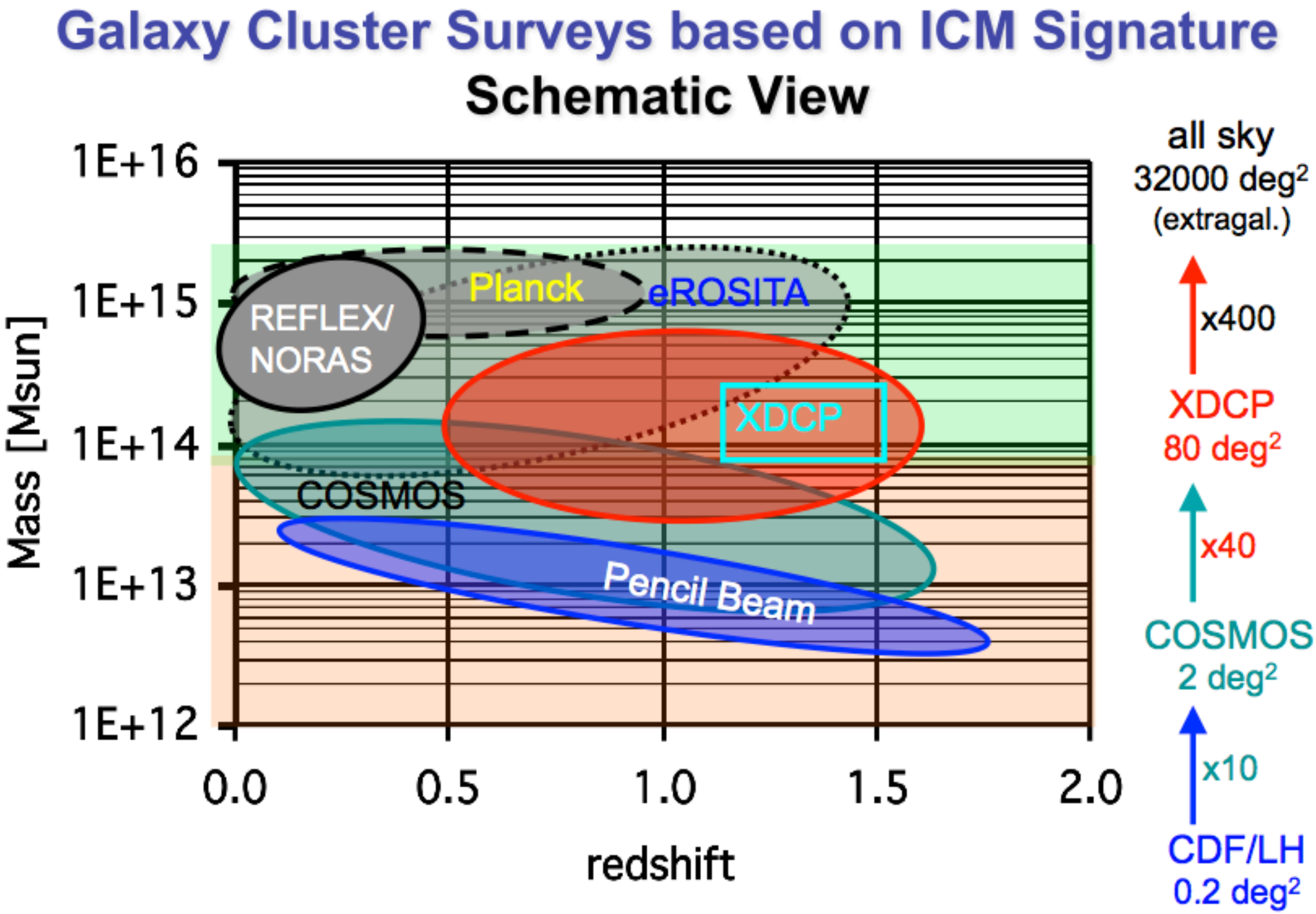

Massive clusters at high-z

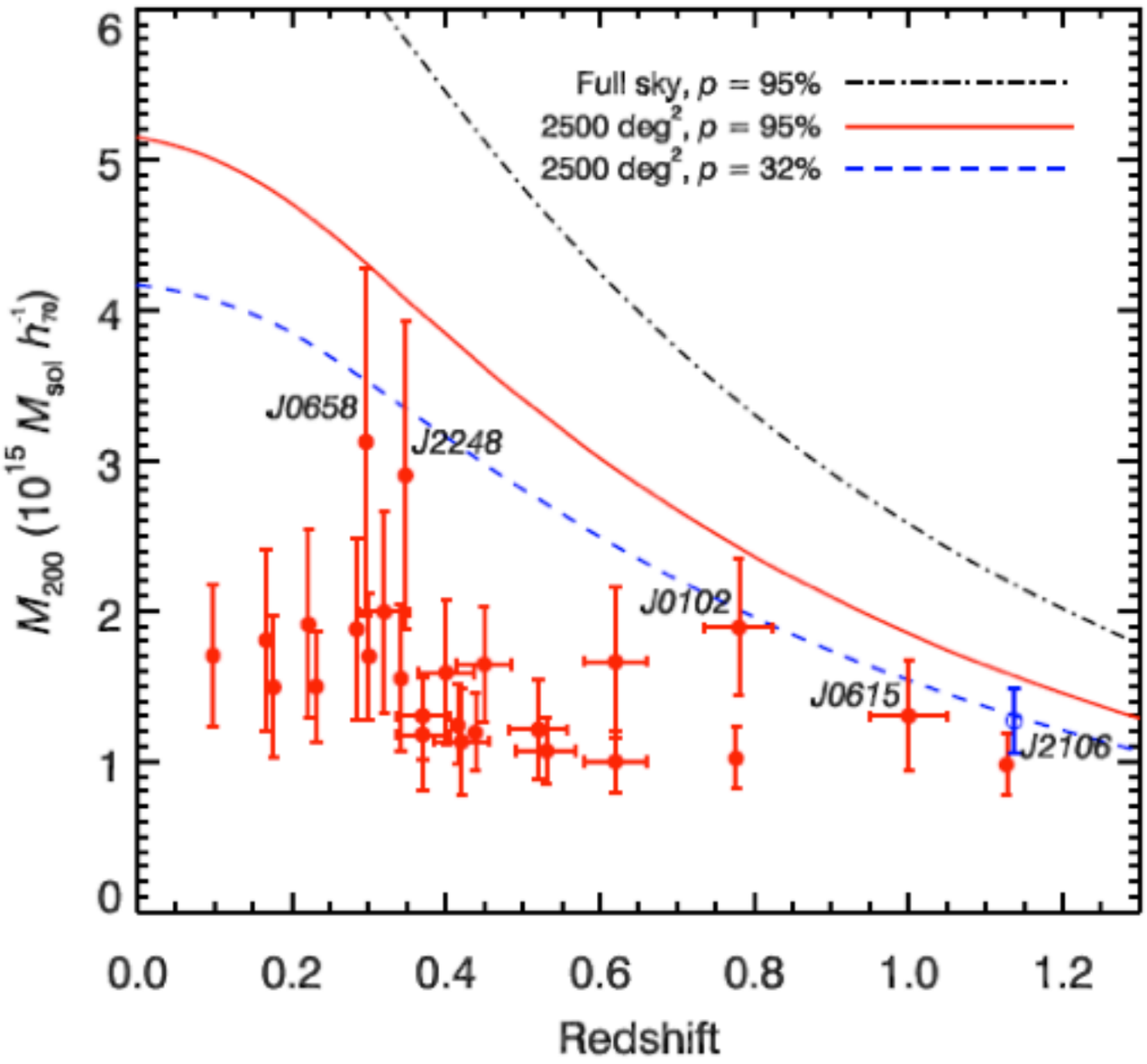

26 SZ clusters from SPT (2500 sq. deg.)
Williamson et al., arXiv:1101.1290

IDCS J1426.5+3508
at z=1.75

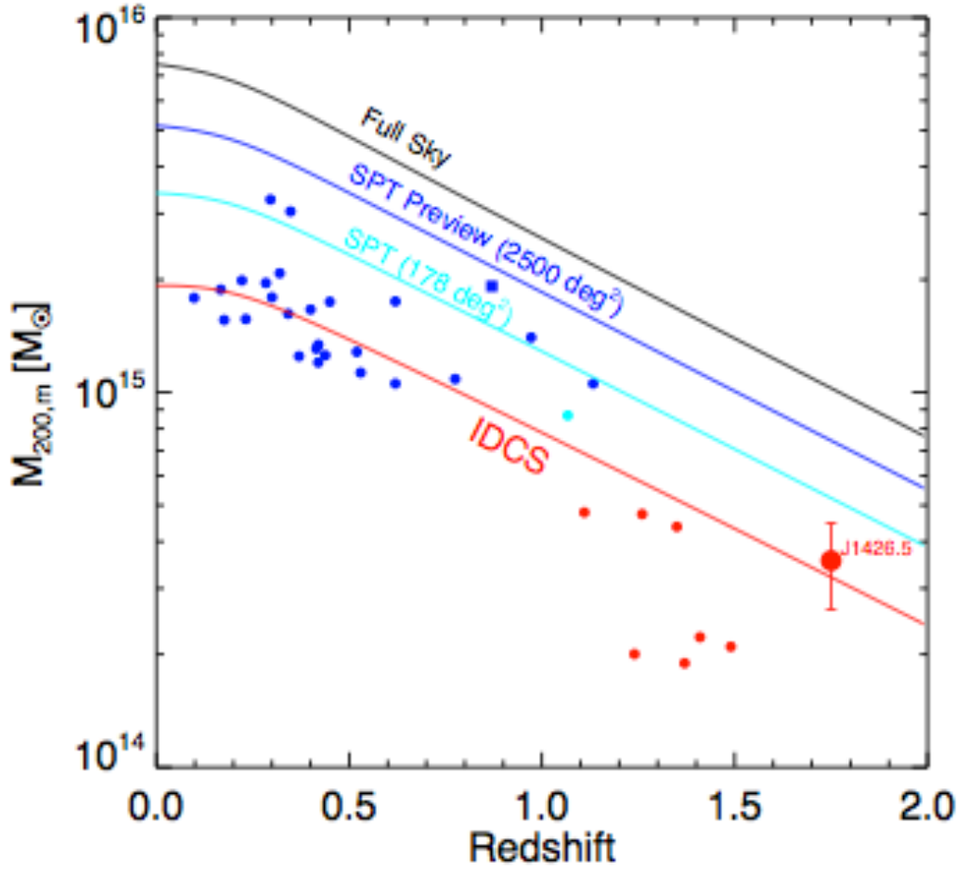

All z>1 clusters, solid lines are 95% exclusion boundaries.

Massive clusters at high-z

expected mass and redshift range of the most massive cluster included in different survey areas

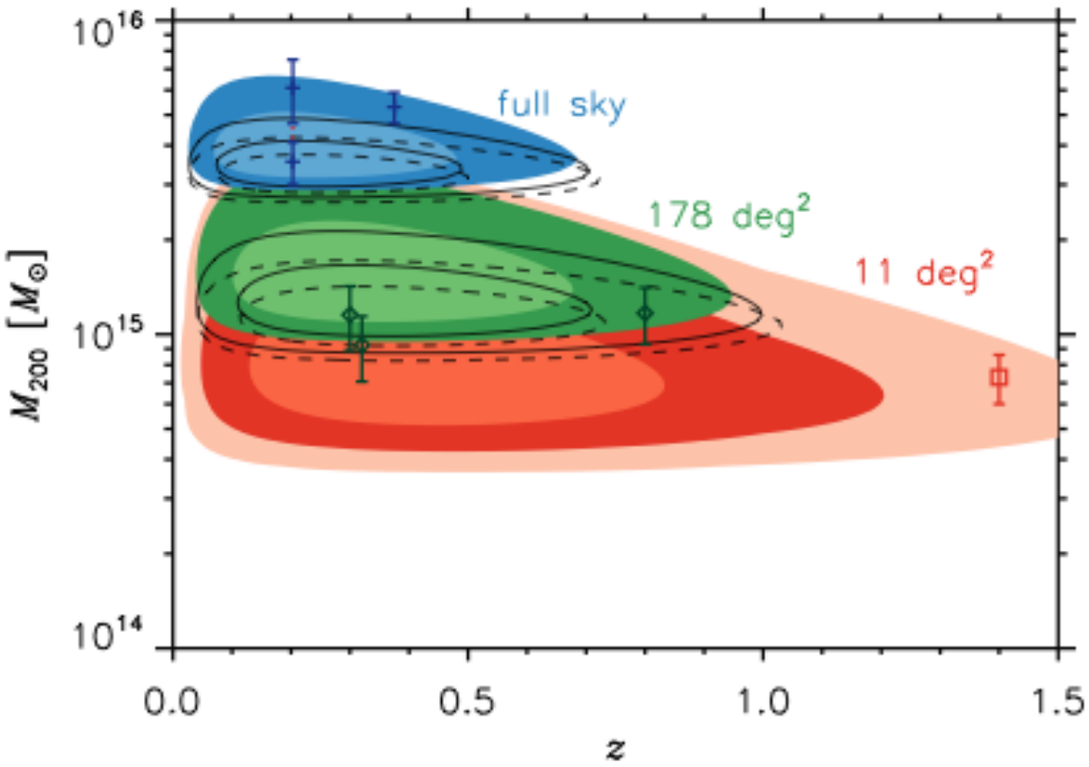

M_{max}~4x10^{15}M_{sun}

full sky = 41253 square degrees

Source: Holz & Perlmutter 2010

expected full sky abundances (in log10) of galaxy clusters with a mass ≥$M_{200,min}$ at redshift ≥z_{min}

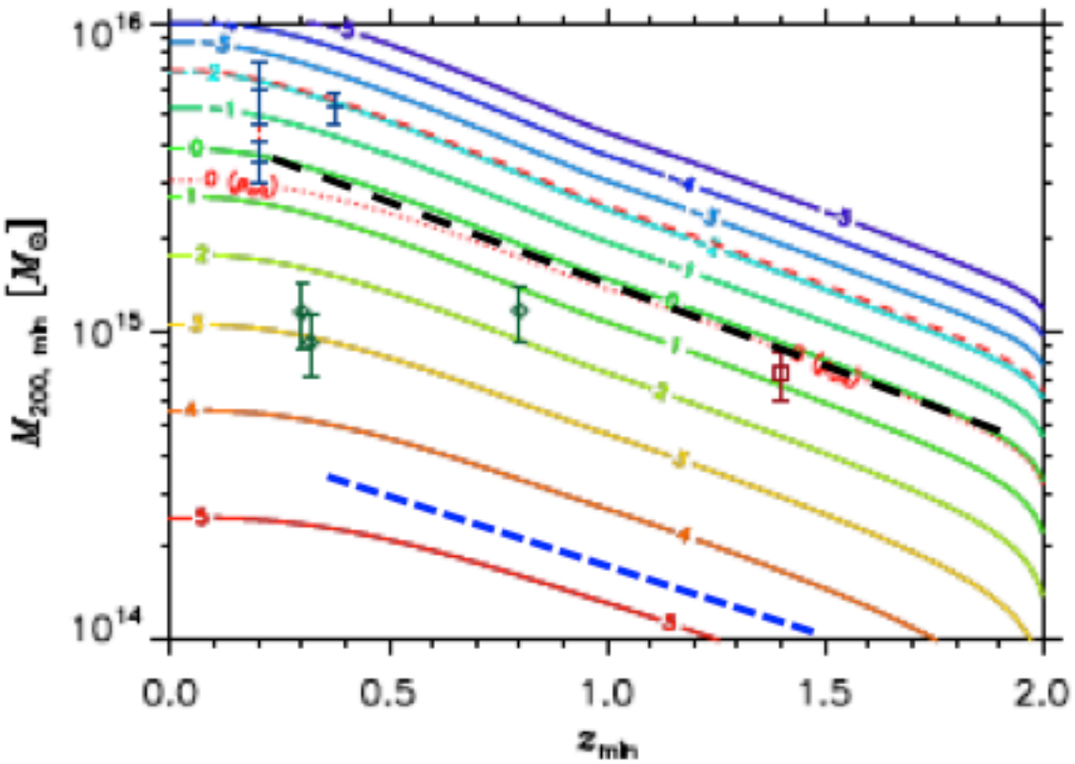

~1 object in the whole sky (---)

~1 object per square degree (---)

Photometry of clusters

The Color-Magnitude-Diagram (CMD)

as basic tool for the study of galaxy evolution in galaxy clusters

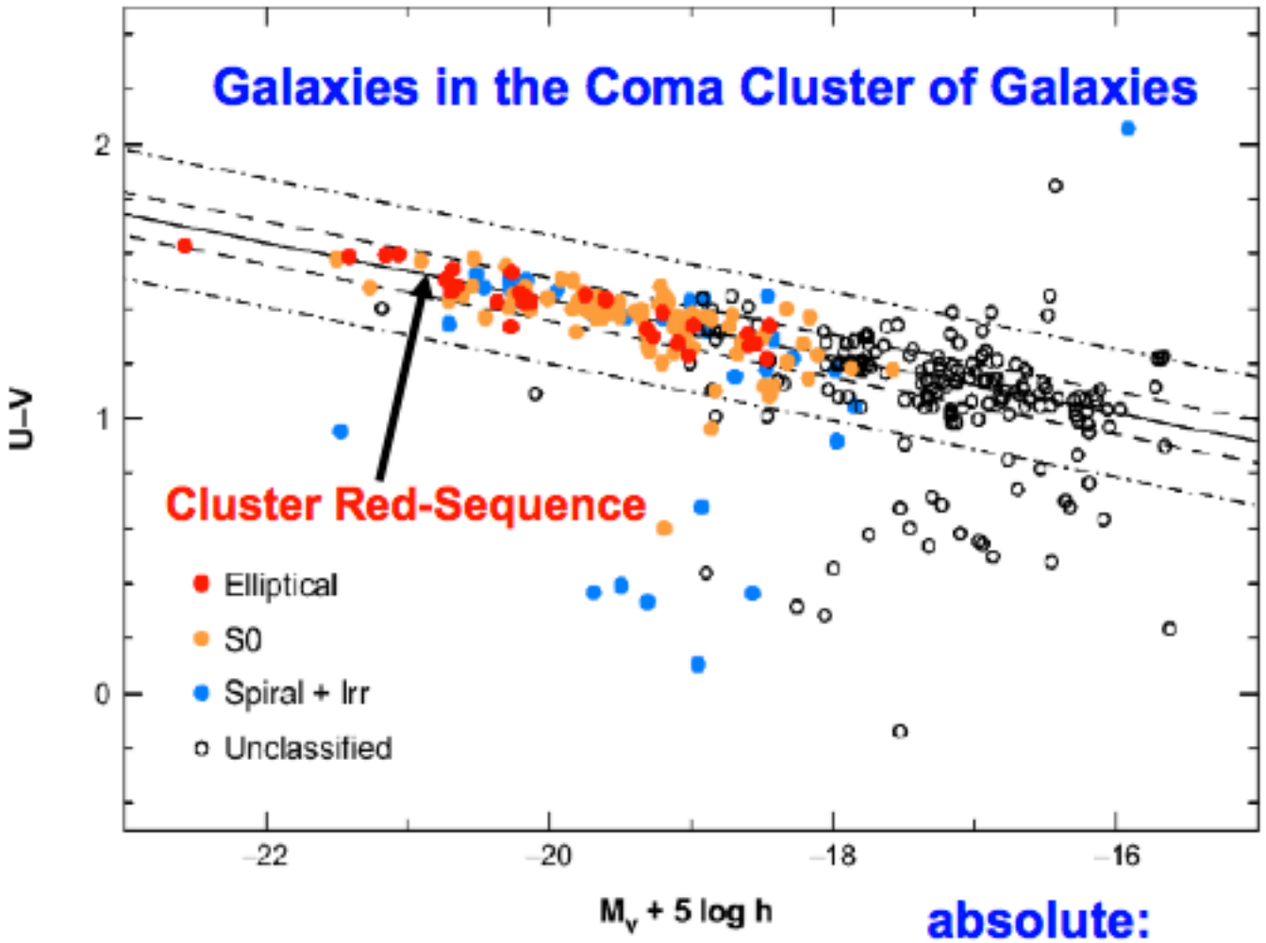

the **brighter** a galaxy
→the farther on the **left**

the **redder** a galaxy
→the farther **up** in the CMD

the pronounced locus (Häufungslinie) of early-type galaxies (E+S0) is called **Red-Sequence**

Source: Bower et al. 1989

absolute: M_X-M_Y vs M_Y

observed: m_X-m_Y vs m_Y

M=M($M_{stellar}$, Z, SF-history, dust,…)

m=m(**z**, $\mathbf{K_{cor}}$, $M_{stellar}$, Z, SF-history, dust,…)

Red sequence technique

- a pronounced red-sequence in the CMD is a basic cluster characteristic and is present for basically all known clusters up to high-z

- red-sequence galaxies selected with appropriate color-cuts in the CMD give a high contrast of cluster members relative to background/ foreground galaxies (interlopers)

- the identification of a red-sequence with an appropriate filter combination is an efficient method for the optical/IR search for distant clusters or the photometric confirmation of X-ray selected candidates

- the redshift evolution of the red-sequence in the CMD (mean color/ zero point, RS slope, scatter) is a powerful tool to study early-type galaxy formation and evolution in clusters

- the homogeneous color properties and redshift evolution of the RS sequence galaxies suggest a common underlying formation mechanism

Galaxies in the red sequence

Credit: Barrientos et al., RCS survey

Figure 2: IJK colour composite image of the field centred on RCS0439.6-2905. North is up and East to the left. This image shows approximately the central 1.1 × 1.1 Mpc.

Galaxies in the red sequence

Credit: Barrientos et al., RCS survey

Figure 2: IJK colour comp and East to the left. This i

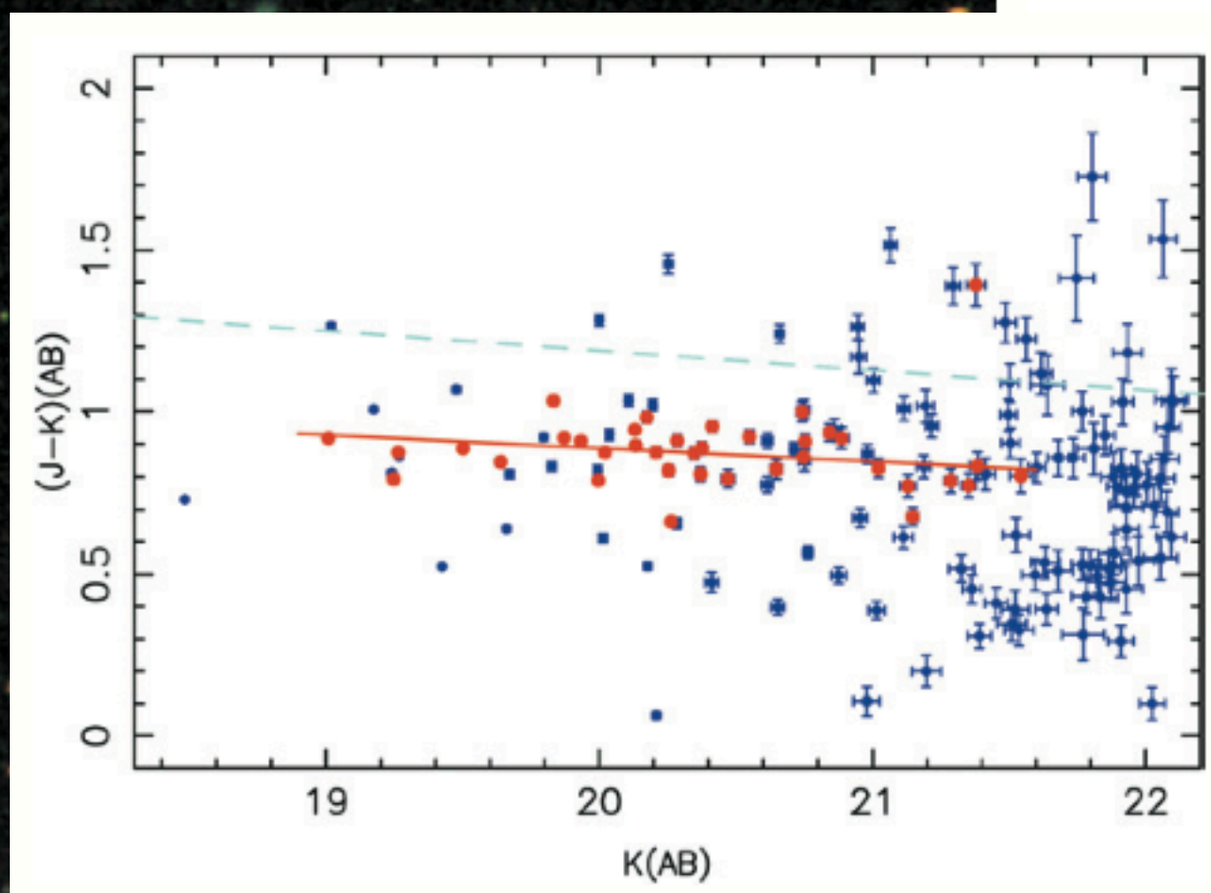

Figure 3: IR colour-magnitude diagram in the field of RCS0439.6-2905. All the objects are included and shown as filled circles. The morphologically selected E/S0 galaxies are shown as open circles. These galaxies define a tight sequence, similar to that found in local clusters. The solid line shows the best fit to the sequence of E/S0 galaxies in the cluster. The broken line corresponds to the colour-magnitude relation for the E/S0 galaxies in Coma cluster redshifted to z = 0.97.

Red sequence technique

The red-sequence technique is uses the fact that all galaxy clusters, however they were discovered, possess a population of galaxies which exhibit a tight relationship in colour--magnitude space, the red-sequence.

The red-sequence method involves constructing many colour slices from the survey data and searching for overdensities of galaxies in these slices. Once significant overdensities are found, the slice containing the peak signal for the overdensity gives the cluster candidate's most probable redshift.

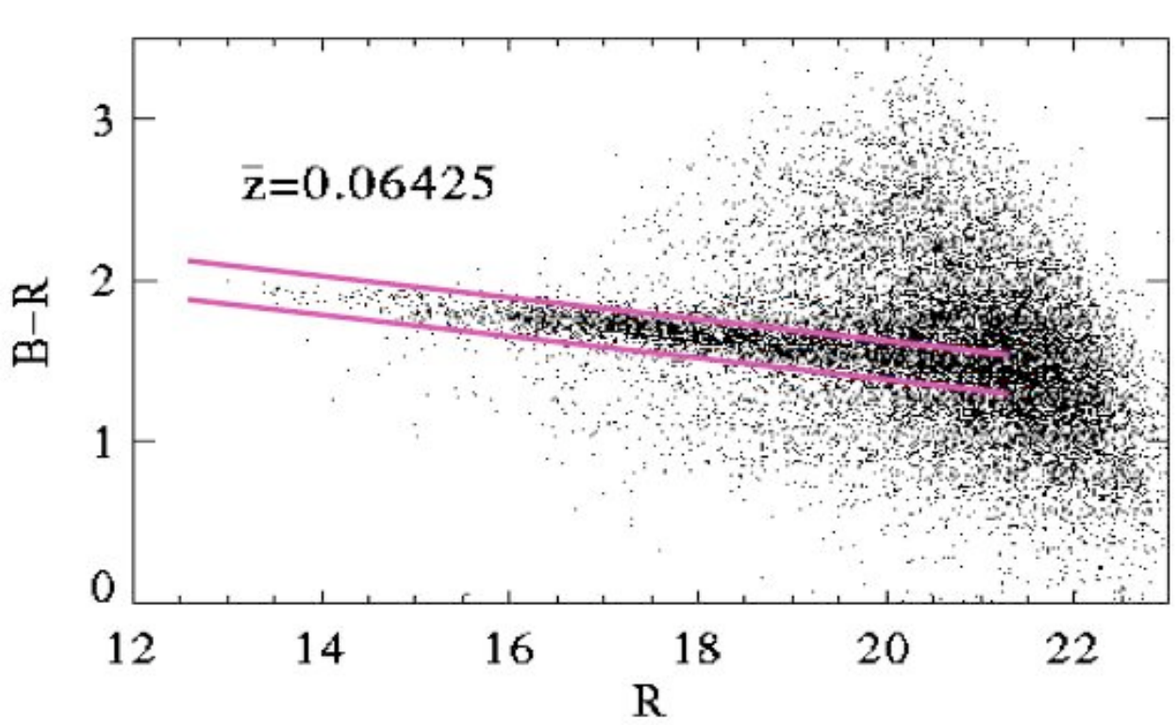

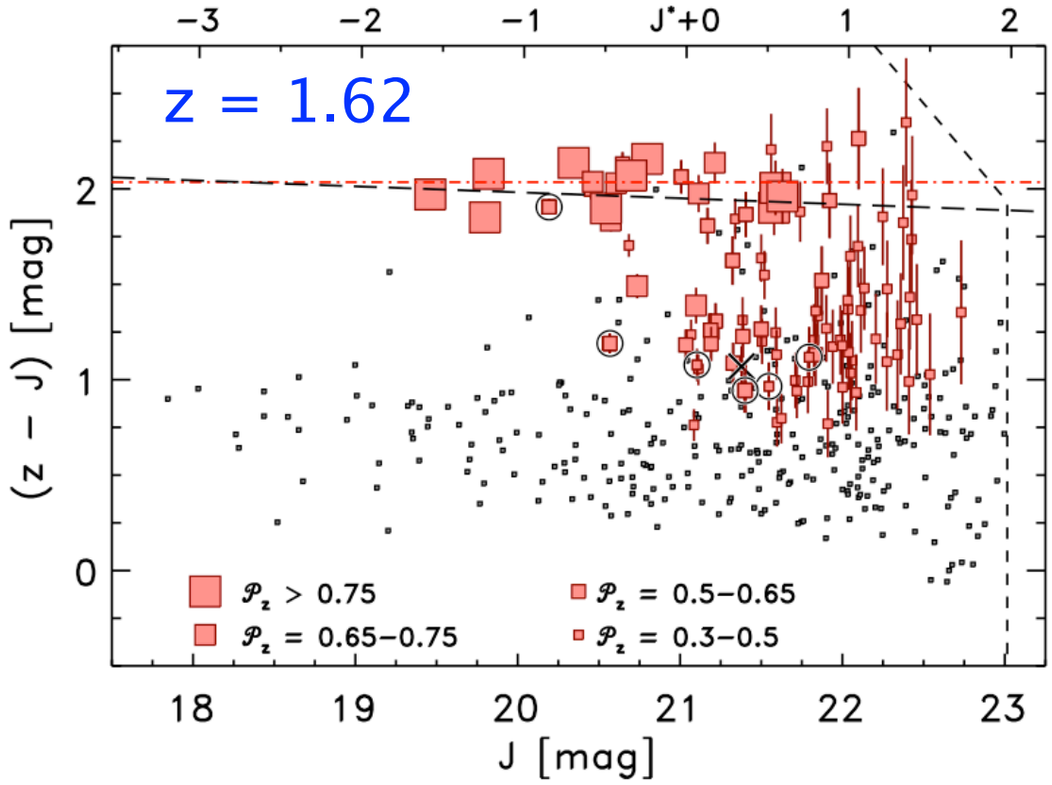

Requires only 2 filters: inexpensive

Red sequence technique

The Clusters Red-Sequence at high-z

in absolute magnitudes looks (almost) like the local RS

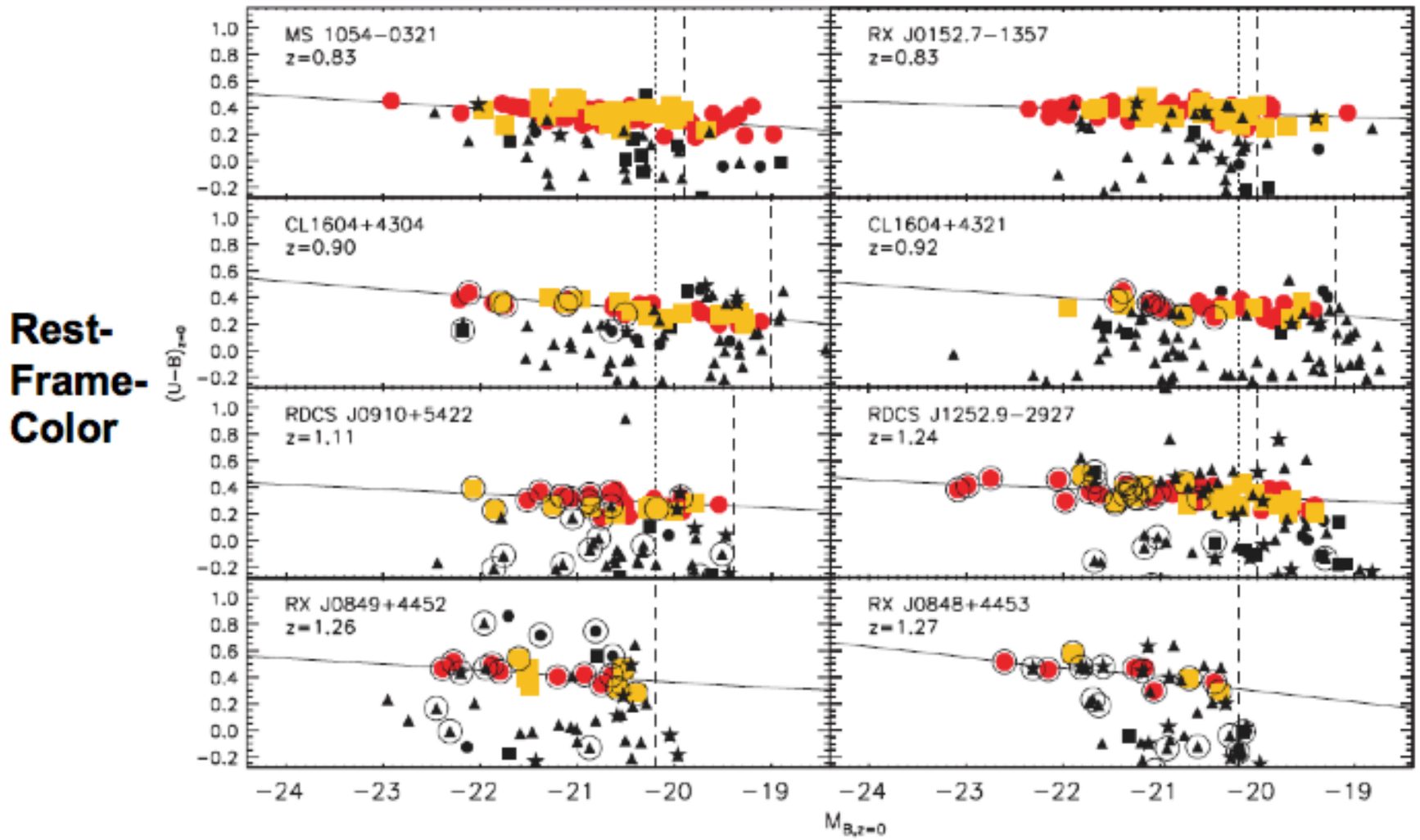

Source: Mei et al. 2009

Red-sequence Cluster Survey

The Red Sequence Cluster Survey 2

- The Red Sequence Cluster Survey 2 (RCS2) is the largest systematic search for galaxy clusters ever undertaken. Using the square-degree imager, MegaCam, on the CFHT, we are imaging nearly 1000 square degrees of sky in three filters (*g'*, *r'*, *z'*) in order to find clusters out to z~1. The project uses the ubiquitous red-sequence of cluster early-type galaxies to identify clusters with a well-understood selection function. This technique was used with great success in the 90 square degree *R* and *z* survey, RCS1.

Main Science Goals: (RCS2)

- Constrain cosmological parameters
  Ω_m (to ~0.03), σ_8 (to ~0.05), w
- create a sample of ~150 strong lenses
- cluster evolution
- weak lensing, cosmic shear (wide/shallow)
- a very large sample of photo-z
  (useful $0.1<z<0.7$)

Cluster sample:

- optimized for z~0.1 to 1.0;

Total number of clusters (useful for cosmology) expected: ~ 15,000 ($>\sim 2\times10^{14}$)

Clusters Richness

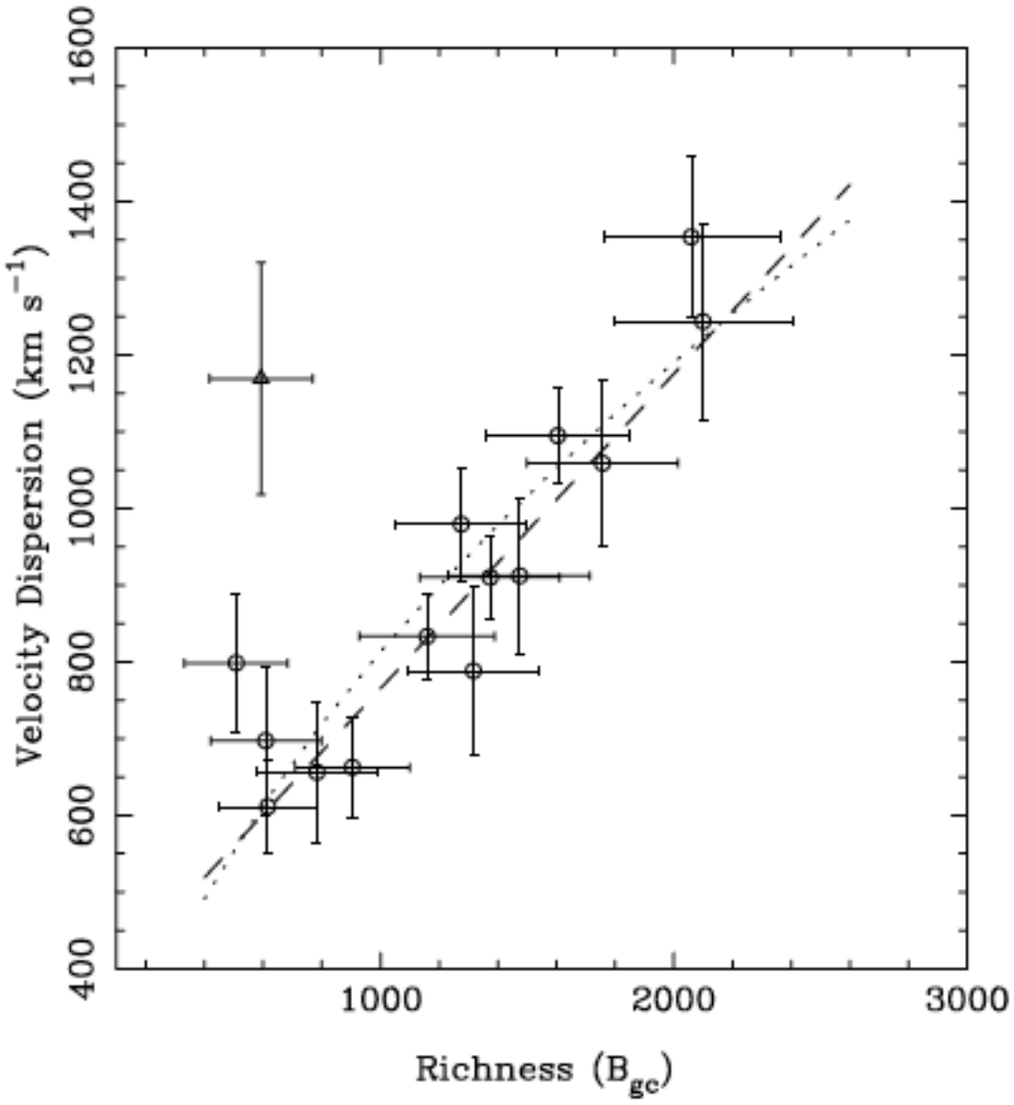

Clusters in optical surveys are selected on the basis of richness, which depends on the number of galaxies observed within a certain projected radius from the cluster center.

$$\frac{M_{200}}{10^{14}h^{-1}\,M_\odot} = (1.42 \pm 0.08)\left(\frac{N_{200}}{20}\right)^{1.16\pm0.09}.$$

Yee & Ellingson 2003

Velocity dispersion

Velocity dispersion is the optical analog of X-ray temperature.

Observationally: $\sigma^2 = (1.0 \pm 0.1)\, k_B\, T_{lum} / \mu\, m_p$

But this gas-mass weighted temperature, $T_{lum,}$ is typically ~20% higher than X-ray spectroscopic temperature (non-gravitational effects? clumping?)

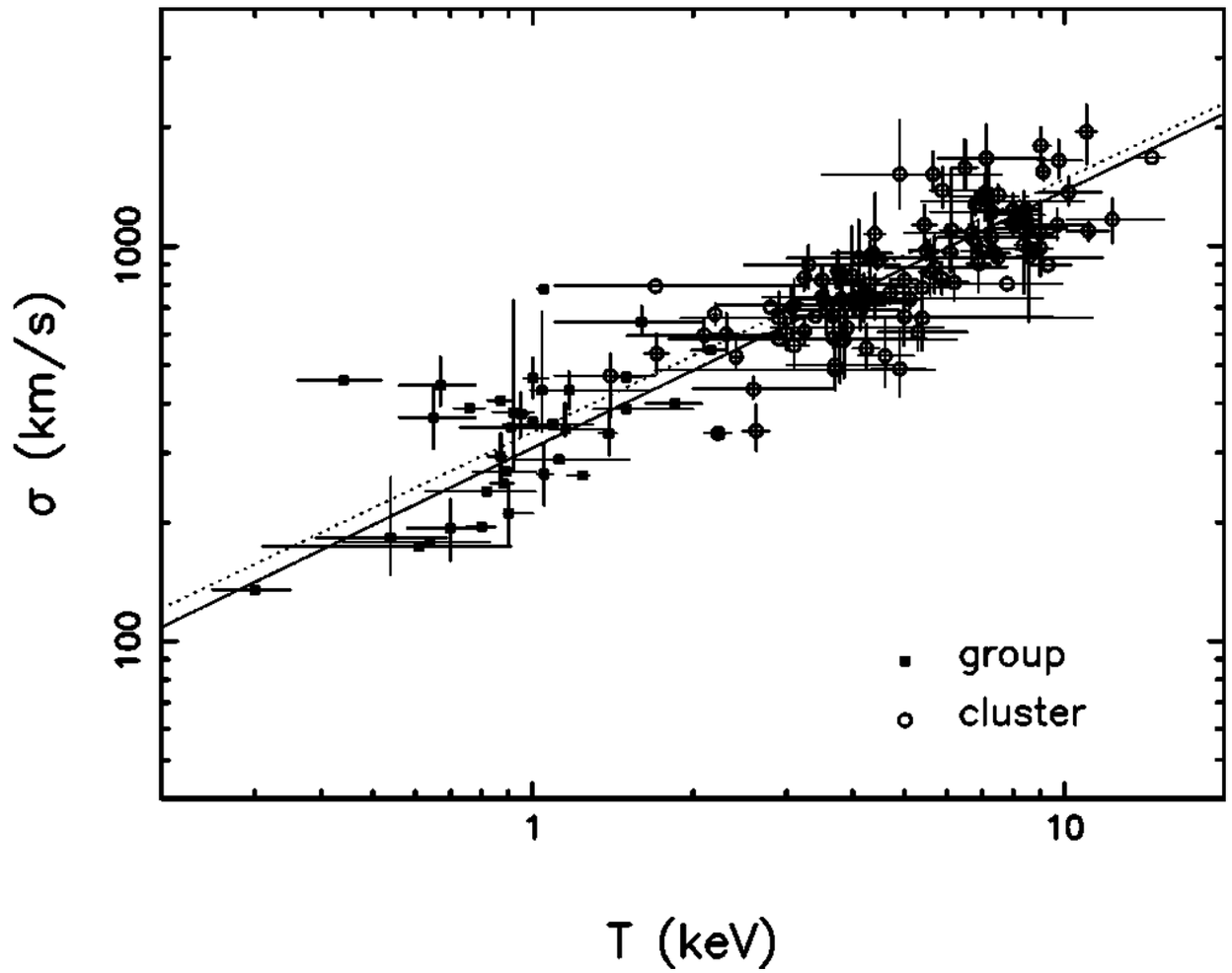

Measuring velocity dispersion

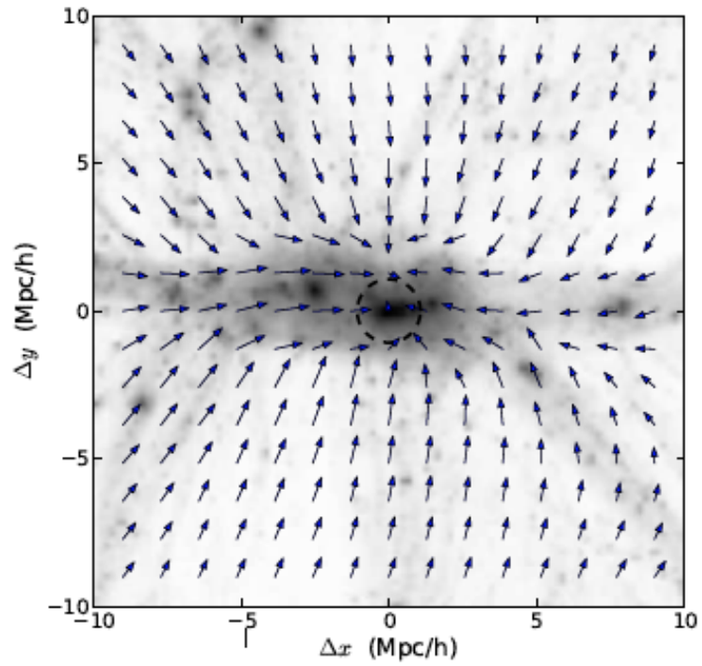

The velocity field traces the filamentary substructure

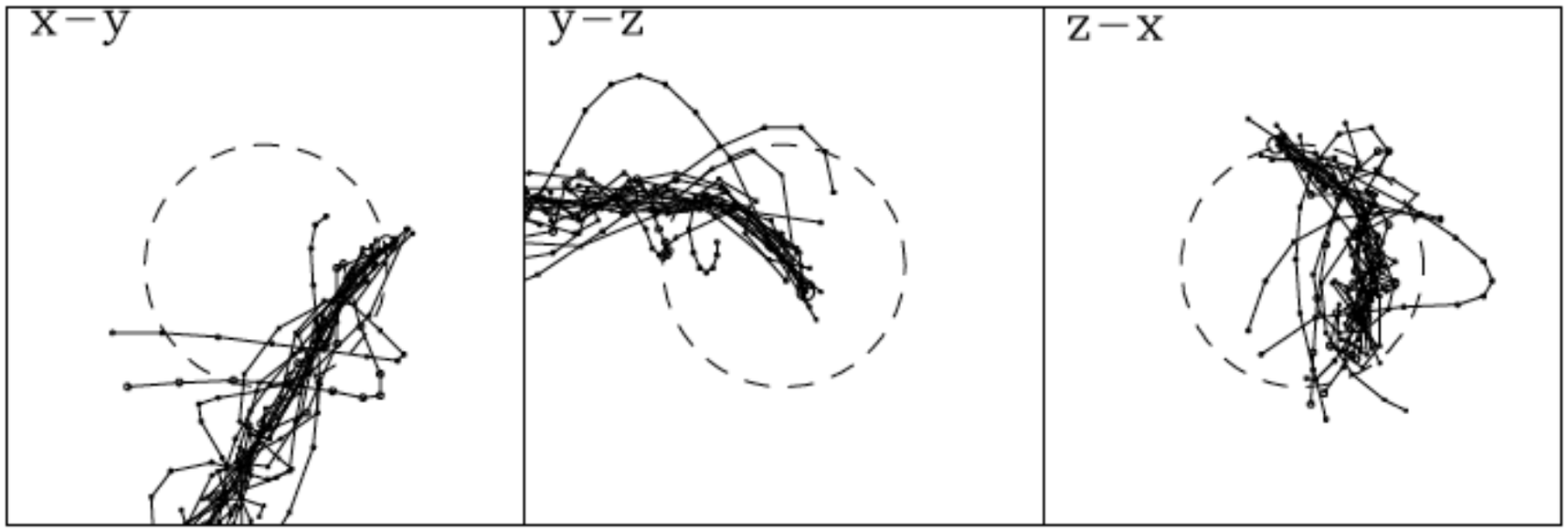

Persistence of substructures (simulations by White, Cohn & Smit 2010)

Example: dynamical mass

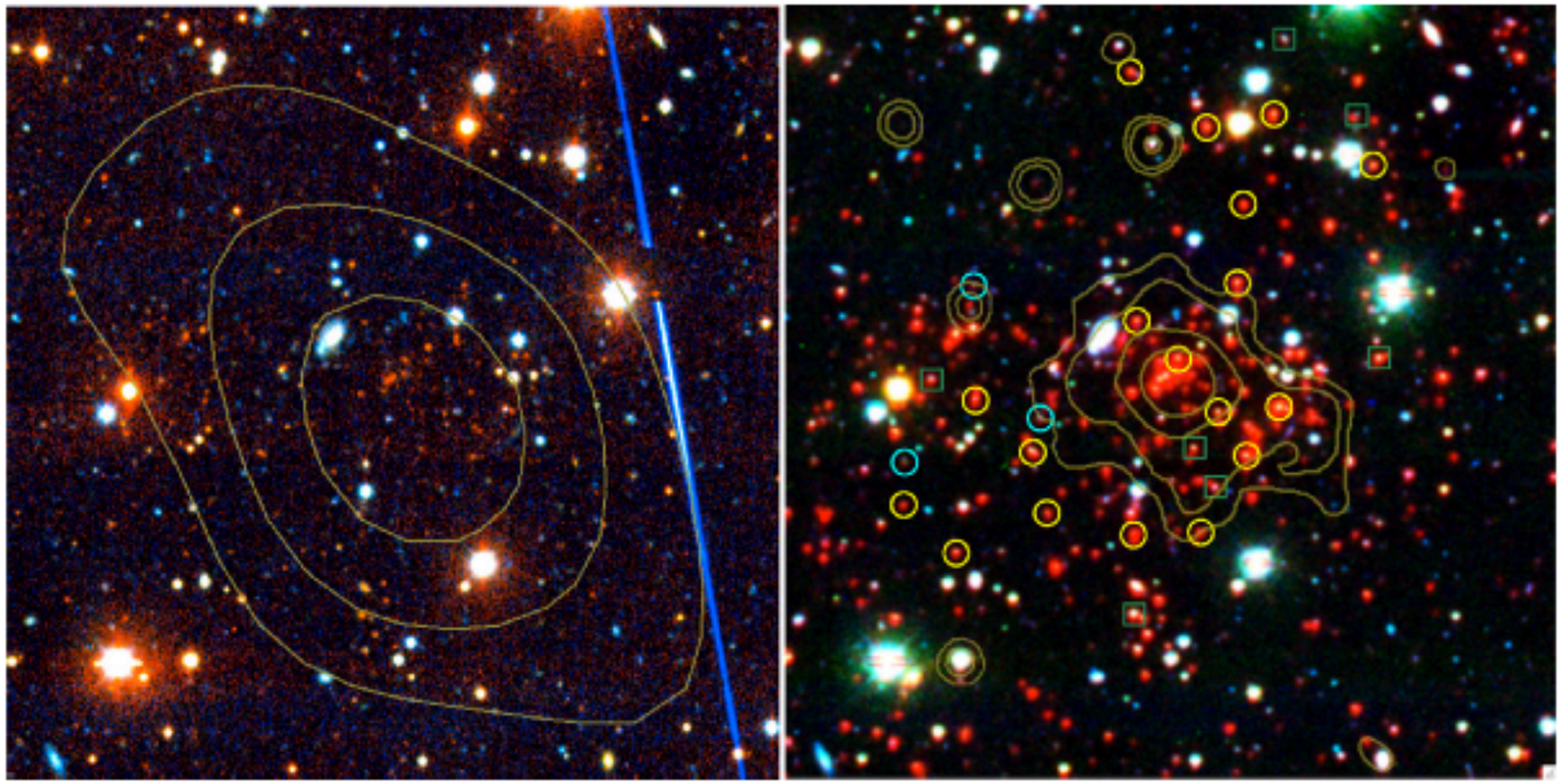

Figure 1. Left: optical $4' \times 4'$ color image (grz) of SPT-CL J0546-5345, with SZE significance contours overlaid (S/N = 2, 4, and 6). Right: false color optical (ri)+IRAC (3.6 μm) image of SPT-CL J0546-5345, with *Chandra* X-ray contours overlaid (0.25, 0.4, 0.85, and 1.6 counts per $2'' \times 2''$ pixel per 55.6 ks in the 0.5–2 keV band). North is up, east is to the left. Due to its high angular resolution, *Chandra* is able to resolve substructure to the SW, which may be evidence of a possible merger. These images highlight the importance of IRAC imaging in studying the galaxies in high-redshift, optically faint clusters. Spectroscopic early-type (late-type) members are indicated with yellow (cyan) circles. Green squares show the spectroscopic non-members.

Example: dynamical mass

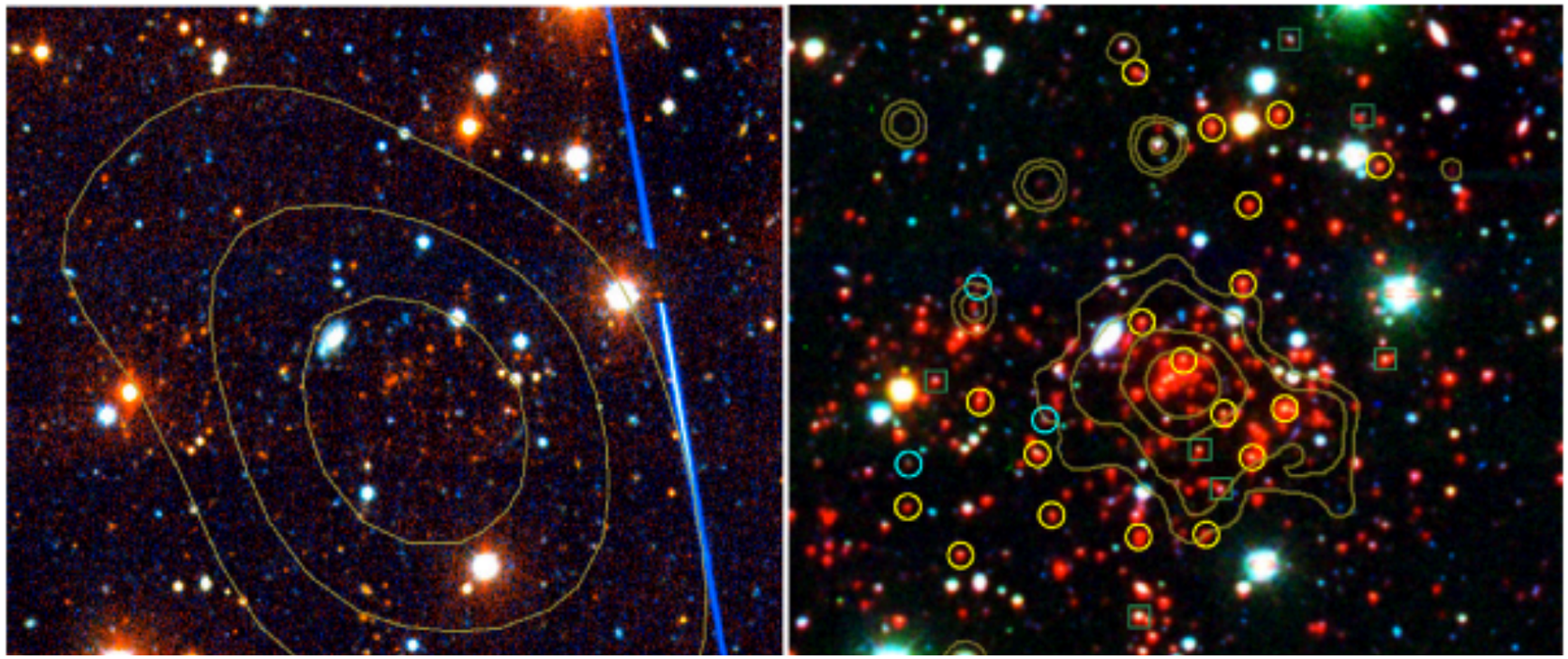

Comparison of Mass Measurements for SPT-CL J0546-5345

Mass Type	Proxy	Measurement	Units	Mass Scaling Relation	M_{200}[a,b] ($10^{14}\,M_\odot$)
Dispersion	**Biweight**	1179^{+232}_{-167}	km s^{-1}	σ–M_{200}(Evrard et al. 2008)	$\mathbf{10.4^{+6.1}_{-4.4}}$
	Gapper	1170^{+240}_{-128}	km s^{-1}	σ–M_{200} (Evrard et al. 2008)	$10.1^{+6.2}_{-3.3}$
	Std deviation	1138^{+205}_{-132}	km s^{-1}	σ–M_{200} (Evrard et al. 2008)	$9.3^{+5.0}_{-3.2}$
X-ray	$\boldsymbol{Y_X}$	5.3 ± 1.0	$\times 10^{14}\,M_\odot$keV	Y_X–M_{500} (Vikhlinin et al. 2009)	$\mathbf{8.23 \pm 1.21}$
	T_X	$7.5^{+1.7}_{-1.1}$	keV	T_X–M_{500} (Vikhlinin et al. 2009)	8.11 ± 1.89
SZE	$\boldsymbol{Y_{SZ}}$	3.5 ± 0.6	$\times 10^{14}\,M_\odot$keV	Y_{SZ}–M_{500} (A10)	$\mathbf{7.19 \pm 1.51}$
	S/N at 150 GHz	7.69		ξ–M_{500} (V10)	$5.03 \pm 1.13 \pm 0.77$
Richness	$\boldsymbol{N_{200}}$	80 ± 31	Galaxies	N_{200}–M_{200} (H10)	$\mathbf{8.5 \pm 5.7 \pm 2.5}$
	N_{gal}	66 ± 7	Galaxies	N_{gal}–M_{200} (H10)	$9.2 \pm 4.9 \pm 2.7$
Best	**Combined**				$\mathbf{7.95 \pm 0.92}$

Figure 1 (ri)+IR 0.5–2 ke possible (late-typ

optical in the e of a y-type

Radio observation of clusters

While the thermal gas emitting in X-rays is present in all clusters, the detection of extended radio emission only in ~10% of the systems indicates that the non-thermal plasma is not a common property of galaxy clusters. Non-thermal emissions over ~1 Mpc scales are present only in the most massive merging systems.

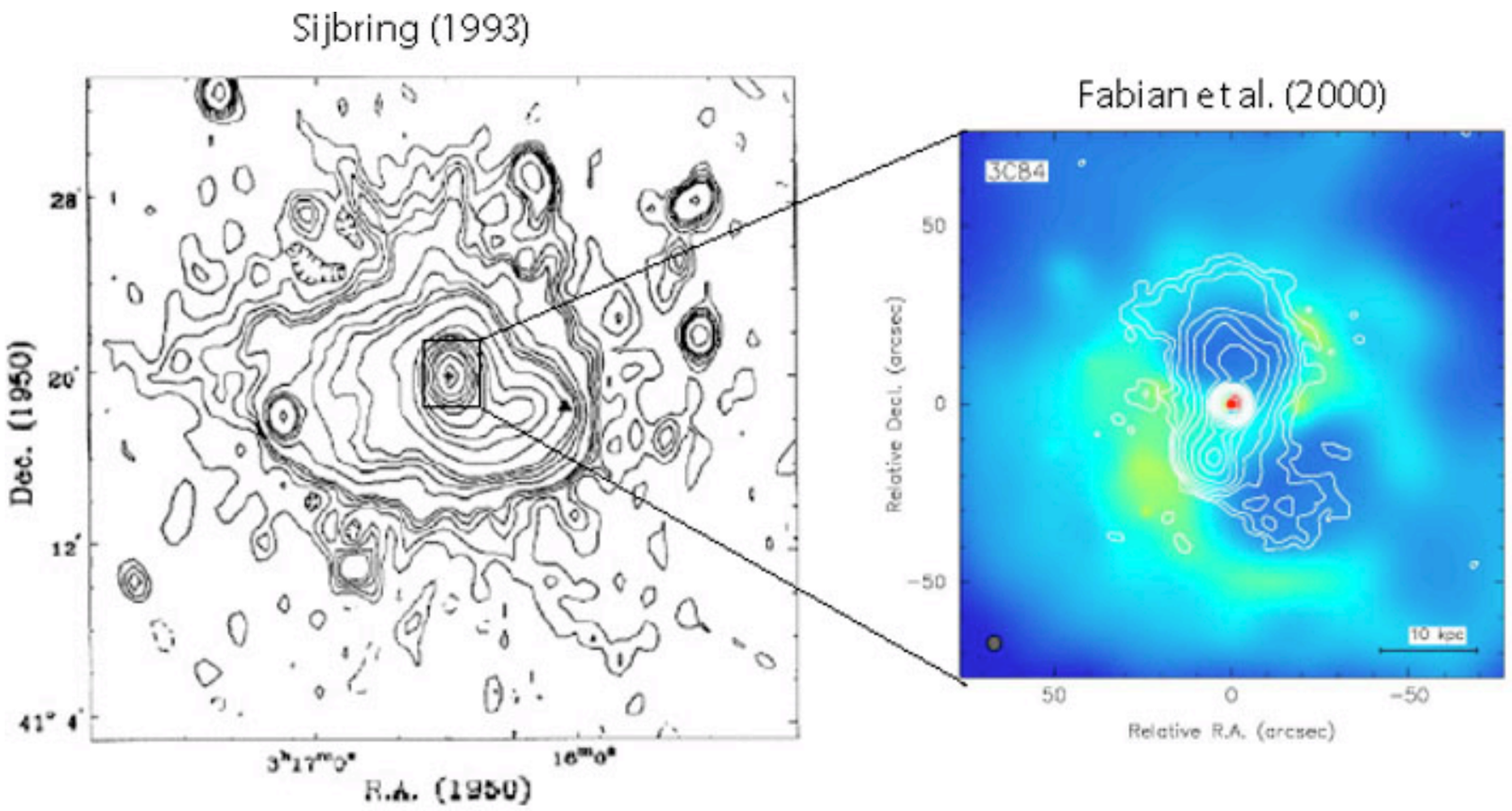

327 MHz map of the mini-halo in the Perseus cluster (z = 0.018).

Radio phenomenology

- radio relics: $\alpha_\nu \sim 1 - 2.5$, where $j_\nu \propto \nu^{-\alpha_\nu}$
  - radio relic bubble: aged radio cocoon, steep spectrum
  - radio phoenix: shock-revived bubble that has already faded out of the radio window → *adiabatic compression?*
  - radio gischt: irregular morphology, at cluster periphery ($<$ Mpc), in some cases coincident with weak X-ray shock, polarized → *diffusive shock acceleration (Fermi I)?*
- radio halos: centrally located, regular morphology, $\alpha_\nu \sim 1 - 1.5$, unpolarized → volume filling radio emission
  - giant radio halos: occur in merging clusters, $>$ 1 Mpc-sized, morphology similar to X-rays
  - radio mini halos: occur in cool core clusters, few times 100 kpc in size, emission extends over cool core

Radio phenomenology

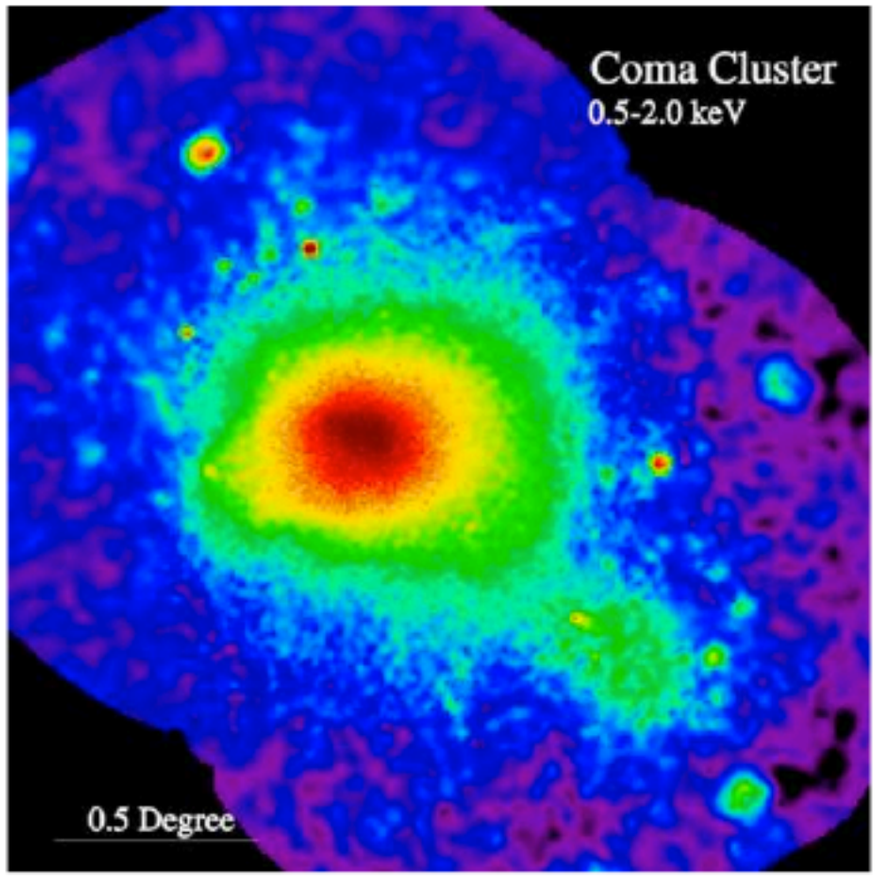

thermal X-ray emission

(Snowden/MPE/ROSAT)

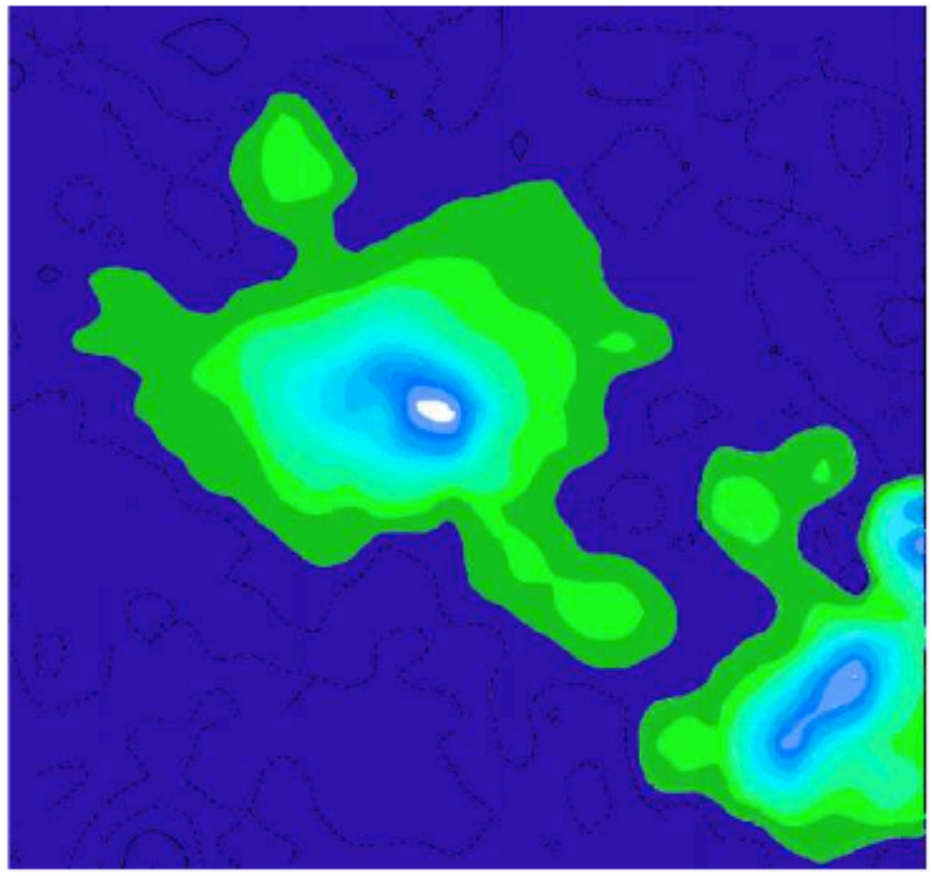

radio synchrotron emission

(Deiss/Effelsberg)

Radio global properties

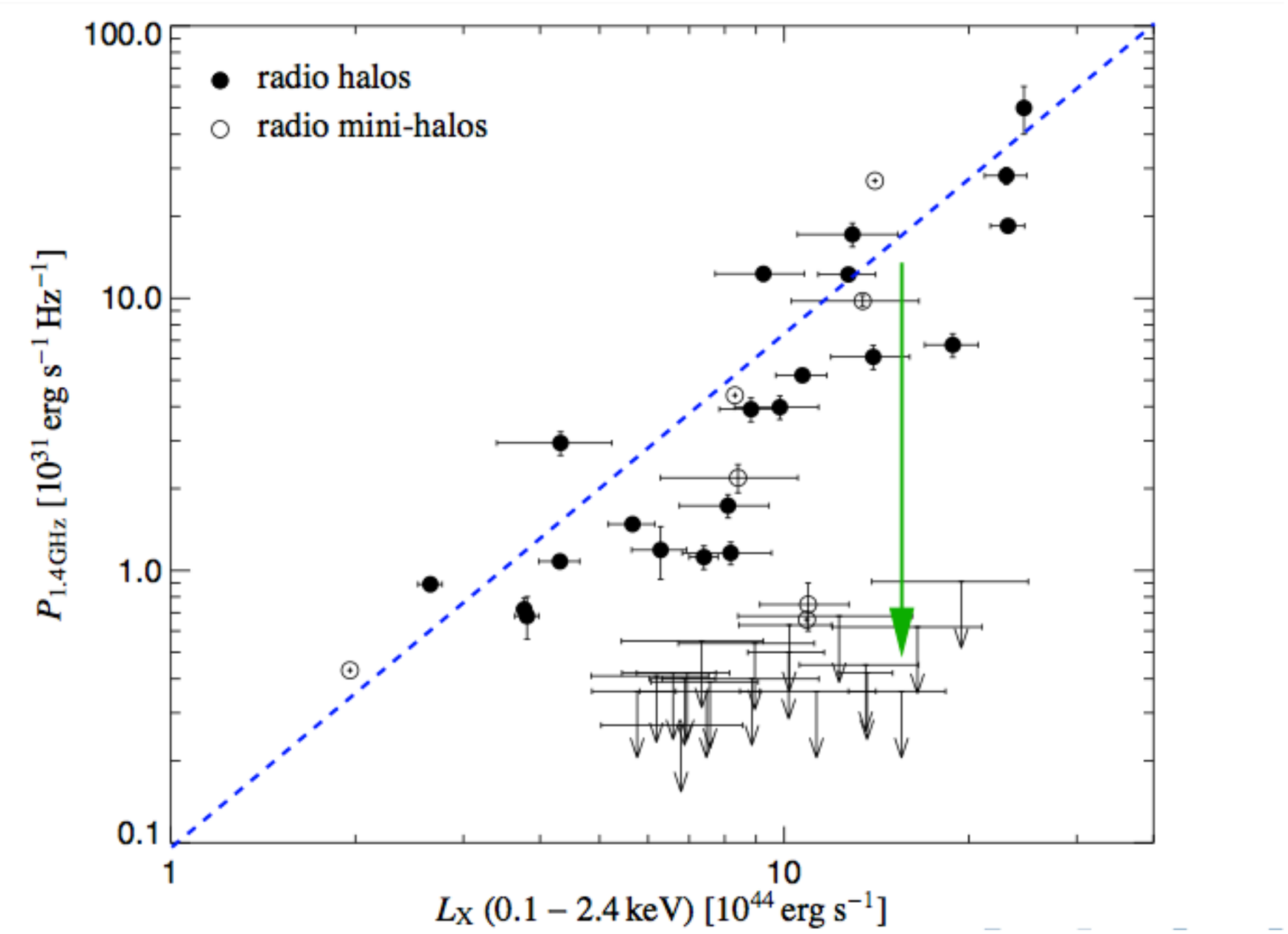

Radio global properties

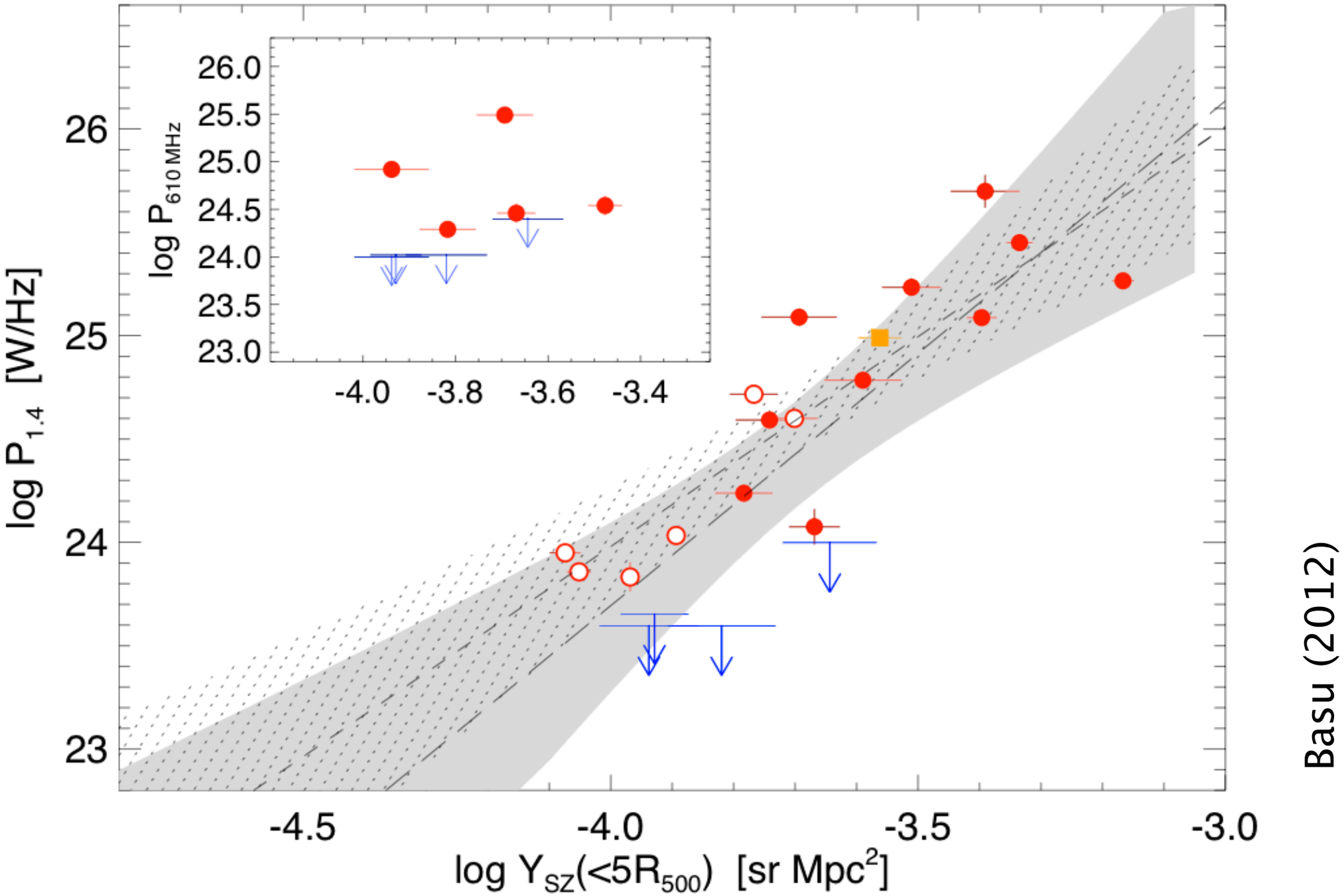

Radio halo – mass correlation

$$P_{1.4} \propto M_H^{2.1\pm0.3} \propto M_{\rm vir}^{3.4\pm0.4}$$

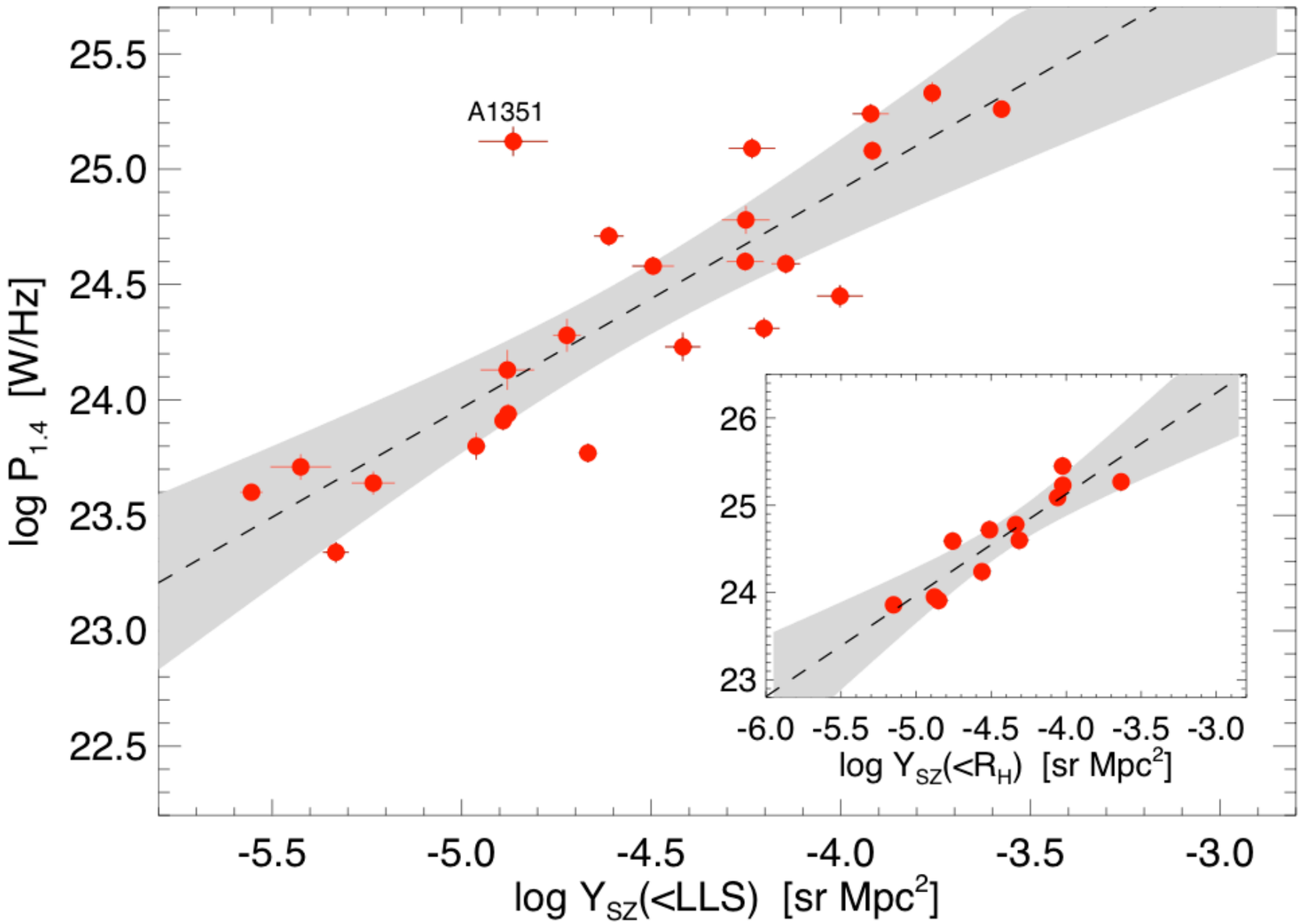

Basu (2012)

Non-thermal γ-rays from clusters

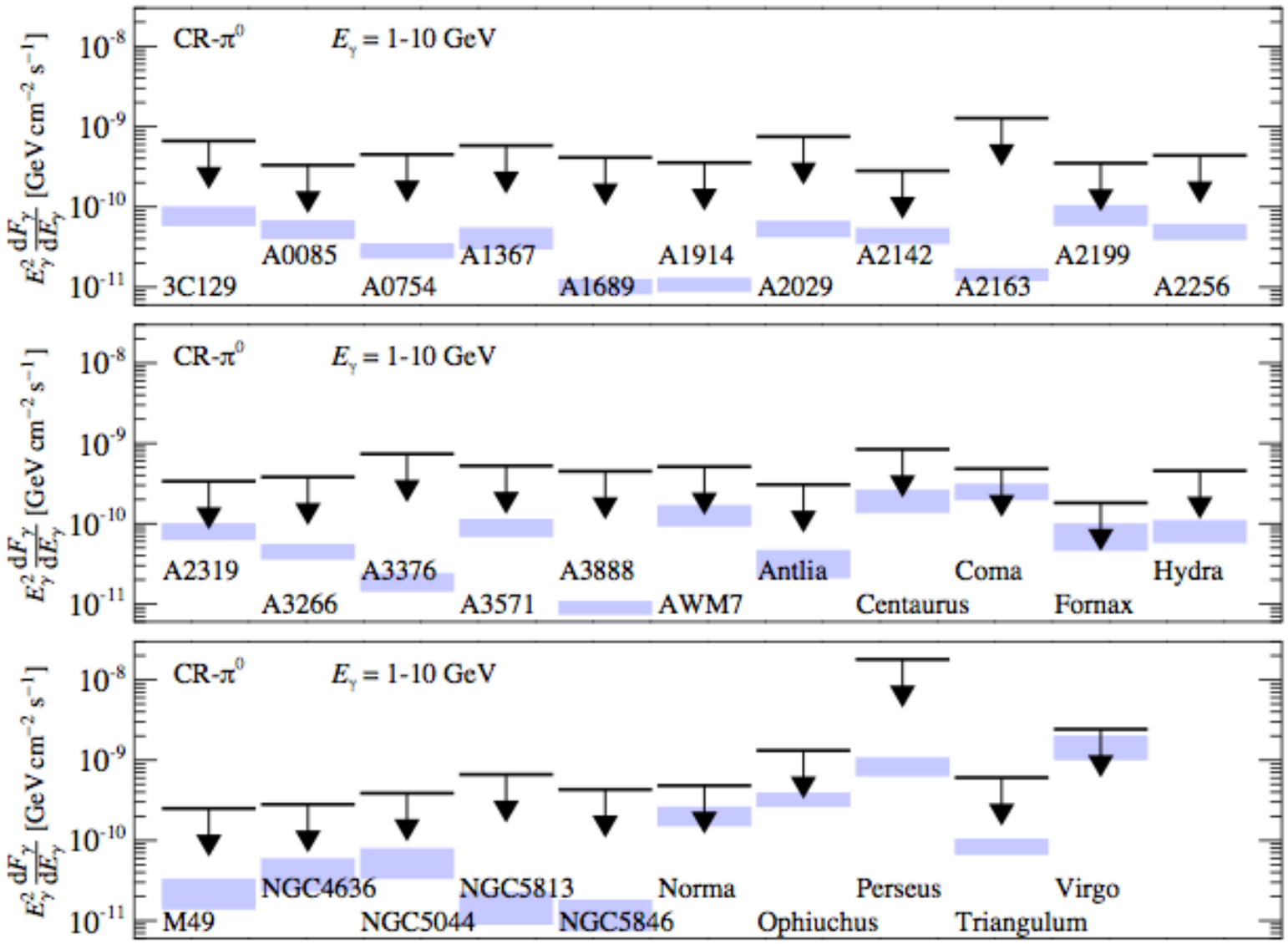

Prediction from Hadronic Model (Pinzke et al. 2011)